Structural Engineering and Mechanics, *Vol. 70, No. 5 (2019) 601-621*
DOI: https://doi.org/10.12989/sem.2019.70.5.601

Vibration of sandwich plates considering elastic foundation, temperature change and FGM faces

Behzad Mohammadzadeh[*1,2], Eunsoo Choi[**3b] and Dongkyun Kim[3c]

[1]*Department of Landscape Architecture and Rural System Engineering, Seoul National University, Seoul, 08826, South Korea*
[2]*Research Institute of Agriculture and Life Sciences, Seoul National University, Seoul 08826, Korea*
[3]*Department of Civil Engineering, Hongik University, Seoul 04066, Republic of Korea*

(Received November 14, 2018, Revised February 12, 2019, Accepted March 11, 2019)

Abstract. This study presents a comprehensive nonlinear dynamic approach to investigate the linear and nonlinear vibration of sandwich plates fabricated from functionally graded materials (FGMs) resting on an elastic foundation. Higher-order shear deformation theory and Hamilton's principle are employed to obtain governing equations. The Runge–Kutta method is employed together with the commercially available mathematical software MAPLE 14 to solve the set of nonlinear dynamic governing equations. Method validity is evaluated by comparing the results of this study and those of previous research. Good agreement is achieved. The effects of temperature change on frequencies are investigated considering various temperatures and various volume fraction index values, N. As the temperature increased, the plate frequency decreased, whereas with increasing N, the plate frequency increased. The effects of the side-to-thickness ratio, c/h, on natural frequencies were investigated. With increasing c/h, the frequencies increased nonlinearly. The effects of foundation stiffness on nonlinear vibration of the sandwich plate were also studied. Backbone curves presenting the variation of maximum displacement with respect to plate frequency are presented to provide insight into the nonlinear vibration and dynamic behavior of FGM sandwich plates.

Keywords: nonlinear vibration; dynamics; sandwich plate; functionally graded materials; frequency analysis; higher order shear deformation theory; Runge-Kutta method

1. Introduction

Beams and plates are structural components which are relatively small in a specific dimension (Ghayesh and Farokhi 2015, Ghayesh *et al*. 2016, Ghayesh *et al*. 2013, Farokhi *et al*. 2013). Beams are formulated as one-dimensional elements or line structural elements (Ghayesh 2018, Ghayesh *et al.* 2017, Farokhi and Ghayesh 2015, Ghayesh *et al*. 2013, Farokhi *et al*. 2017) while plates are represented as two-dimensional or surface structural elements (Farokhi and Ghayesh 2015, Ghayesh *et al*. 2013, Farokhi and Ghayesh 2018). Plates have been widely used as key components in various structures, such as vehicles, containers, and spacecraft (Mohammadzadeh, and Noh 2014, Ebrahimi and Heidari 2018, Mohammadzadeh, and Noh 2016, Mohammadzadeh *et al*. 2018). Sandwich plates possess advantages of light-weight, significant rigidity, fatigue resistance, and excellent vibration properties; hence, they have attracted considerable attention for use in engineering applications (Ahmadi 2018, Bouderba *et al*. 2016, Elmossouess *et al*. 2017, Choi *et al*. 2018). They are categorized as specific batches of laminates and are generally formed with two thin face sheets and a thick core (Belarbi *et al*. 2016, Daoudii and Adim 2017, Feli and Jalilian 2017, Sharivat *et al*. 2015). The face sheets have the role of carrying planar and bending loads, while the core resists against compressive stresses and transfers shear loads (Mohammadzadeh 2016). In 1984, Japanese scientists mixed ceramic and metal powders into a graded profile to create a new generation of engineering materials, so-called functionally graded materials (FGMs) (Rajabi *et al*. 2016). High fracture toughness is a specific characteristic of the metallic part, while the ceramic part is characterized by high thermal resistance (Rajasekaran 2013). The volume fraction index, N, dictates the variation of material properties in a specific direction. Material properties like the modulus of elasticity E, Poisson's ratio υ, material density ρ, and shear modulus of elasticity G, gradually change in the intended direction. FGMs were developed by combining the forms of fibers, particulates, whiskers, or platelets of advanced materials (Heydari *et al*. 2015). Considerable attention have been attracted to FGMs because of their superior characteristics in comparison to conventional materials. Because of the wide use of FGMs in industries and structures such as spacecraft heat shields, heat exchanger tubes, fusion reactors, and airplane fuselages, numerous studies have investigated FGM plates (Ninh and Bich 2016). Some studies employed first-order shear deformation theory to deal with static analysis, free vibration, or buckling of FGMs (El Meiche *et al*. 2011). Other methods including the third-order shear deformation and three-dimensional elasticity have also been considered to investigate FGM structures (Li *et al*. 2009). A nonlinear analysis of sandwich plates with FGM face sheets resting

∗Co-Corresponding author, Ph.D.
E-mail: Behzad.alb@gmail.com
∗∗Co-Corresponding author, Professor
E-mail: eunsoochoi@hongik.ac.kr

http://www.techno-press.com/journals/sem&subpage=7
ISSN: 1225-4568 (Print), 1598-6217 (Online)

on an elastic foundation in thermal environments was performed in (Wang and Shen 2011).

Transverse shear deformation was included in the kinematics of composite laminates because the thickness significantly affects the behavior of composite laminates (Yang *et al*. 2013, Soni *et al*. 2017). To account for shear effects, two theories can be employed: first-order shear deformation theory (FSDT) and higher-order shear deformation theory (HSDT). FSDT cannot correctly represent through-thickness distribution and requires shear coefficients to correct the corresponding strain energy terms. Besides, the effect of warping, which is important for thick plates, is not included in FSDT. To overcome the disadvantages of FSDT, HSDT has been applied because it considers the through-thickness displacement as the higher-order polynomial functions (Demasi 2013, Nguyen *et al*. 2017).

Dynamic and nonlinear analyses of structural elements have attracted the attentions as in practical applications the structure frequently subject to dynamic loads while suffering both the geometrical and material nonlinearities (Ghayesh 2018, Gholipour *et al*. 2015, Ghayesh *et al*. 2013, Farokhi and Ghayesh 2018). The vibration analysis of FGMs structural components has attracted attention during the last decade because of the increased interests in using FGMs for the design and construction of structures (Wang and Zu 2018, Wang 2018, Wang and Zu 2017). However, the literature on the frequency analysis of FGM sandwich plates is very limited. Some studies have employed FSDT (Zhu *et al*. 2018), second-order shear deformation theory (Shahrierdi *et al*. 2011), and HSDT-based new approaches (Vafakhah and Navayi Neva 2019) to perform mechanical vibration analysis of FGM sandwich plates while some studied the thermal vibration of FGM sandwich plates [Alibeigloo 2017, Wang *et al*. 2018] and presented a new theory for free vibration analysis of bi-directional FGMs (Zamani Nejad *et al.* 2017). The nonlinear vibration of a functionally graded graphene platelet-reinforced composite with a rectangular shape and different edge conditions considering geometric nonlinearity, rotary inertia, and transverse shear deformation was investigated by (Gholami and Ansari 2018). By use of Hamilton's principle and the variational differential quadrature technique, the weak form of discretized nonlinear equations of motion was obtained and solved by a multistep numerical approach based on the Galerkin method, time-periodic discretization method, and pseudo-arc-length continuation. (Natarajan and Manickam 2012) investigated the free flexural vibration behavior of FGM sandwich plates by employing the QUAD-8 shear flexible element developed based on the HSDT. They investigated the effects of the gradient index and the plate aspect ratio on the plate global and local responses. Despite several studies on the vibration analysis of FGM plates, sandwich plates and laminated composites (Ghayesh 2018, Ghayesh *et al.* 2017, Ghayesh *et al*. 2018, Wang *et al*. 2019, Wang and Yang 2017, Wang and Zu 2018, Wang *et al*. 2013,), the effects of temperature changes, complex boundary conditions, and changes in material properties have been rarely taken into consideration (Wang and Zu 2017, Wang *et al*. 2016).

Wang *et al*. (2018), investigated the free thermal vibration of FGM cylindrical shells containing porosities. They considered the even and uneven distribution of porosities as well as three thermal load types uniform, linear and nonlinear temperature rise. A modified power-law formulation was employed for a description of the material properties of FGM plates in thickness-direction. Love's shell theory was employed to formulate the strain displacement equations while the Rayleigh-Ritz method was used to calculate the natural frequencies of the system. In another study (Wang and Zu 2017), the vibration analysis of FGM rectangular plates was conducted considering the thermal environment, porosities and geometric nonlinearity based on the von Kármán nonlinear plate theory. For this purpose, the equation of motion of the system was obtained by using the D'Alembert's principle taking into account the thermal effect and longitudinal speed. The Galerkin method was utilized to reduce the partial differential equation of motion to a set of ordinary differential equations, and solved by the method of harmonic balance.

Having all above it can be mentioned that dealing with analytical analysis of composite laminated structural elements considering complex conditions and advanced materials are still facing challenges; thus, this study was intended to provide a comprehensive approach considering complex conditions such that any desired material can be specified to the sandwich plate in any desired number of layers through the plate thickness to investigate the plate linear and nonlinear vibrations together with the frequency behavior. Besides, having look at the literature, a few number studies can be found investigating the nonlinear vibration of plates (Wang 2014, Wang *et al*. 2019, Wang *et al*. 2018). Therefore, the need for the providing a comprehensive approach for nonlinear vibration analysis of plates comes up.

In this study, linear and nonlinear vibration analyses of sandwich plates having FGM faces resting on the elastic foundation were performed. In this regard, a comprehensive nonlinear dynamic approach was presented employing higher-order shear deformation theory as well as Hamilton's principal. The effects of temperature change, elastic foundation, and variations in material properties on the linear and nonlinear vibration of sandwich plates were included in the presented approach. This approach was designed so that any order of materials in any number of layers can be considered through the thickness of sandwich plates. This characteristic of the presented approach results in more precise results than other methods because any variation of material through the plate thickness can be modeled without the application of any approximation.

2. Derivation of equation of motion

The concepts and guidelines given in the literature were employed to derive the set of equations of motion of the FGM sandwich plate (Mantari *et al.* 2014, Mohammadzadeh and Noh 2017, Cadou *et al*. 2016), solve the equations (Mohammadzadeh and Noh 2015, Kamil Zur 2018, Mohammadzadeh and Noh 2014, Trinh *et al*. 2018, Mohammadzadeh and Noh 2018), obtain the materialproperties of the face sheets and the core (Choi *et al*. 2018, Arunkumar *et al*. 2018, Choi *et al*. 2018) and interpret the results (Ruocco *et al*. 2018, Ngyuen *et al*. 2016, Wang and Zhu 2017).

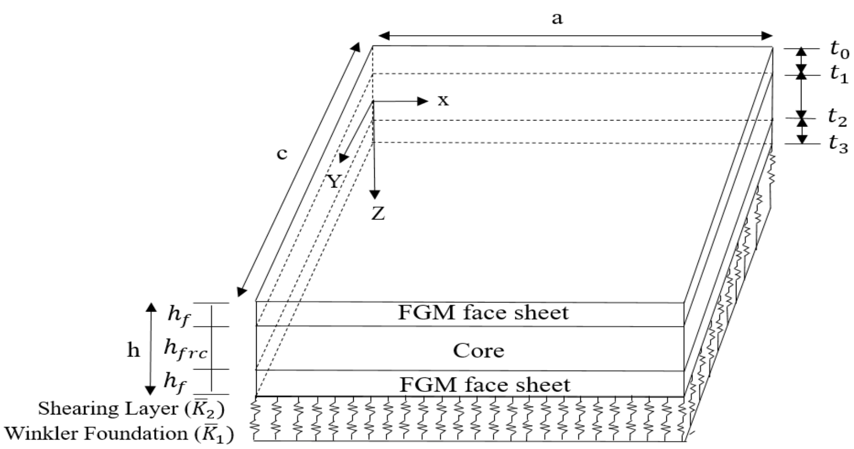

Fig. 1 Illustration of sandwich plate

This study considered a rectangular sandwich plate made of three layers. An FGM is considered for the top and bottom layers, while fiber-reinforced concrete is specified for the core located in the middle. The parameters 'a', 'c' and 'h' denote the length, width, and thickness of the plate, respectively. An illustration of a typical sandwich plate is provided in Fig. 1. It is appropriate to note that the origin of the coordinate system is placed at mid-plane on the corner.

Displacements along the X-direction, length of the plate; Y-direction, the width of the plate; and Z-direction, plate thickness, are U, V, and W, respectively. The mid-plane rotations around the Y-axis and X-axis are indicated by ψ_x and ψ_y, respectively. The displacement components are assumed to have the following form as given in Eq. (1) (Wang and Shen 2011):

$$U = U_0 + Z\left[\psi_x - \frac{4}{3}\left(\frac{Z}{h}\right)^2\left(\psi_x + \frac{\partial W_0}{\partial X}\right)\right], \tag{1a}$$

$$V = V_0 + Z\left[\psi_y - \frac{4}{3}\left(\frac{Z}{h}\right)^2\left(\psi_y + \frac{\partial W_0}{\partial Y}\right)\right], \tag{1b}$$

$$W = W_0 \tag{1c}$$

where the U_0, V_0, W_0, displacements at the mid-surface of the plate, and the rotations ψ_x, and $\psi_y$are uncertain.

The stress is related to strain with respect to the matrix form given in Eq. (2) (Wang *et al*. 2017):

$$\begin{Bmatrix}\sigma_{xx}\\ \sigma_{yy}\\ \sigma_{xy}\end{Bmatrix} = \begin{bmatrix}Q_{11} & Q_{12} & Q_{16}\\ Q_{12} & Q_{22} & Q_{26}\\ Q_{16} & Q_{26} & Q_{66}\end{bmatrix}\begin{Bmatrix}\varepsilon_{xx}\\ \varepsilon_{yy}\\ \varepsilon_{xy}\end{Bmatrix}, \tag{2a}$$

$$\begin{Bmatrix}\sigma_{yz}\\ \sigma_{xz}\end{Bmatrix} = \begin{bmatrix}Q_{44} & Q_{45}\\ Q_{45} & Q_{55}\end{bmatrix}\begin{Bmatrix}\gamma_{yz}\\ \gamma_{xz}\end{Bmatrix}. \tag{2b}$$

Hamilton's principle is employed to derive the equations of motion of the sandwich plate as presented in Eq. (3) (Mohammadzadeh and Noh 2017):

$$\int_0^t (\delta U_{se} + \delta V_{ew} - \delta K_e)dt = 0 \tag{3}$$

The strain energy, external work, and kinetic energy are denoted by U_{se} , δV_{ew}, and δK_e respectively. To provide a better understanding, the extended equation used for derivation of δU is expressed as

$$\begin{aligned}\delta U_{se} = \int_{\Omega_0}\int_{-\frac{h}{2}}^{\frac{h}{2}}\Big\{\Big((\sigma_{xx} + \sigma_x^T)\delta\varepsilon_{xx} + \left(\sigma_{yy} + \sigma_y^T\right)\delta\varepsilon_{yy}\\ + \left(\sigma_{xy} + \sigma_{xy}^T\right)\delta\varepsilon_{xy}\\ + (\sigma_{xz} + \sigma_{xz}^T)\delta\gamma_{xz}\\ + \left(\sigma_{yz} + \sigma_{yz}^T\right)\delta\gamma_{yz}\Big)dz\Big\}dxdy\end{aligned} \tag{4}$$

where the thermal stresses are indicated by σ^T.

The external work is obtained by employing the following equation (Shahrjerdi *et al.* 2011, Mohammadzadeh and Noh 2017):

$$\begin{aligned}\delta V_{ew} = -\int_{\Omega_0}\big[q_x\delta u + q_y\delta v + (q_b + q_t)\delta w\\ + (K_1 W - K_2\nabla^2 W)\delta w\big].\end{aligned} \tag{5}$$

External loads applied on the upper and lower face sheets of the plate are denoted by q_t and q_b, respectively. External forces acting on the plate length and width are denoted by q_x and q_y, respectively. The stiffness of the elastic foundation takes the amount of 10, K_I=10, while that of the shear layer is zero, K_2 = 0. The surface area of the sandwich plate is denoted by Ω_0.

The kinetic energy, δK_e, can be obtained as

$$\begin{aligned}\delta K_e = \int_{\Omega_0}\Big\{\int_{t_1}^{t_0}\rho(Z)\big[(\dot{U}\delta\dot{U}) + (\dot{V}\delta\dot{V}) + (\dot{W}\delta\dot{W})\big]dz\\ + \int_{t_2}^{t_1}\rho_c\big[(\dot{U}\delta\dot{U}) + (\dot{V}\delta\dot{V}) + (\dot{W}\delta\dot{W})\big]dz\\ + \int_{t_3}^{t_2}\rho(Z)\big[(\dot{U}\delta\dot{U}) + (\dot{V}\delta\dot{V})\\ + (\dot{W}\delta\dot{W})\big]dz\Big\}dxdy,\end{aligned} \tag{6a}$$

where superposed dotted variables are related to their time-dependency. Here, t_i is attributed to the layer height. It can be said that each layer is placed between t_{i-1} and t_i. In this regard, as an example, the bottom face sheet is confined between t_2 and t_3 as seen in Fig. 1.

Substituting the Von-Karman strain-displacement relations and mass moments of inertias into Eq. (6a), δK can be rewritten as

$$\begin{aligned}\delta K = \int_{\Omega_0} \Bigg[& I_{0i}(\dot{u}_0\delta\dot{u}_0 + \dot{v}_0\delta\dot{v}_0 + \dot{w}_0\delta\dot{w}_0) \\ & + I_{1i}\big(\dot{U}_0\delta\dot{\psi}_x + \dot{\psi}_x\delta\dot{U}_0 + \dot{V}_0\delta\dot{\psi}_y \\ & + \dot{\psi}_y\delta\dot{V}_0\big) + I_{2i}\big(\dot{\psi}_x\delta\dot{\psi}_x + \dot{\psi}_y\delta\dot{\psi}_y\big) \\ & - \frac{4}{3h^2}I_{3i}\Bigg(\dot{U}_0\delta\dot{\psi}_x + \dot{U}_0\frac{\partial\delta\dot{W}_0}{\partial x} \\ & + \dot{\psi}_x\delta\dot{U}_0 + \frac{\partial\dot{W}_0}{\partial x}\delta\dot{U}_0 + \dot{V}_0\delta\dot{\psi}_y \\ & + \dot{V}_0\frac{\partial\delta\dot{W}_0}{\partial y} + \dot{\psi}_y\delta\dot{V}_0 + \frac{\partial\dot{W}_0}{\partial y}\delta\dot{V}_0\Bigg) \\ & - \frac{4}{3h^2}I_{4i}\Bigg(2\dot{\psi}_x\delta\dot{\psi}_x + \dot{\psi}_x\frac{\partial\delta\dot{W}}{\partial x} \\ & + \frac{\partial\dot{W}_0}{\partial x}\delta\dot{\psi}_x + 2\dot{\psi}_y\delta\dot{\psi}_y + \dot{\psi}_y\frac{\partial\delta\dot{W}}{\partial y} \\ & + \frac{\partial\dot{W}_0}{\partial y}\delta\dot{\psi}_y\Bigg) \\ & + \frac{16}{9h^4}I_{6i}\Bigg(\dot{\psi}_x\delta\dot{\psi}_x + \dot{\psi}_x\frac{\partial\delta\dot{W}_0}{\partial x} \\ & + \frac{\partial\dot{W}_0}{\partial x}\delta\dot{\psi}_x + \frac{\partial\dot{W}_0}{\partial x}\frac{\partial\delta\dot{W}_0}{\partial x} + \dot{\psi}_y\delta\dot{\psi}_y \\ & + \dot{\psi}_y\frac{\partial\delta\dot{W}_0}{\partial y} + \frac{\partial\dot{W}_0}{\partial y}\delta\dot{\psi}_y \\ & + \frac{\partial\dot{W}_0}{\partial y}\frac{\partial\delta\dot{W}_0}{\partial y}\Bigg)\Bigg] dxdy \end{aligned} \tag{6b}$$

The mass moment of inertias of each layer, I_{ji}, is obtained by Eq.(6c) (Mohammadzadeh and Noh 2017):

$$I_{ji} = \int_{t_{i-1}}^{t_i} Z^j\,\rho_i(Z)dz \qquad j = 0,1,2,3,4,5,6, \qquad i = 1,2,3,\ldots \tag{6c}$$

where $\rho_i(Z)$ is the height-dependent density, Z is the height of the layer, sub-index *j* is the order of momentum of inertia, and sub-index *i* denotes the layer limitation number as shown in Fig. 1 by t_0 to t_3. The membrane force N_m, shear force, *Q*, bending moment M_b, higher-order bending moment *P,* and higher-order shear force *R,* are defined as shown in Eq. (7) (Wang and Shen 2011):

$$(N_m, M_b, P) = \int_{-\frac{h}{2}}^{\frac{h}{2}} \sigma(1, Z, Z^3)dz \tag{7a}$$

$$(Q_x, R_x) = \int_{-\frac{h}{2}}^{\frac{h}{2}} \sigma_{xz}(1, Z^2)\,dz \tag{7b}$$

$$\left(Q_y, R_y\right) = \int_{-\frac{h}{2}}^{\frac{h}{2}} \sigma_{yz}(1, Z^2)\,dz \tag{7c}$$

Here, $\bar{N}^T$, $\bar{M}^T$, $\bar{S}^T$ and $\bar{P}^T$ are the thermal forces, moments, and higher-order moments caused by elevated temperature, respectively. They are defined as presented in Eq. (8) (Alibeigloo 2017):

$$\begin{bmatrix} \bar{N}_x^T & \bar{M}_x^T & \bar{P}_x^T \\ \bar{N}_y^T & \bar{M}_y^T & \bar{P}_y^T \\ \bar{N}_{xy}^T & \bar{M}_{xy}^T & \bar{P}_{xy}^T \end{bmatrix} = \sum_{k=1}^{N} \int_{t_{k-1}}^{t_k} \begin{bmatrix} A_x \\ A_y \\ A_{xy} \end{bmatrix}_k (1, Z, Z^3)\Delta T dZ \tag{8a}$$

$$\begin{bmatrix} \bar{S}_x^T \\ \bar{S}_y^T \\ \bar{S}_{xy}^T \end{bmatrix} = \begin{bmatrix} \bar{M}_x^T \\ \bar{M}_y^T \\ M_{xy}^T \end{bmatrix} - \frac{4}{3h^2} \begin{bmatrix} \bar{P}_x^T \\ P_y^T \\ P_{xy}^T \end{bmatrix} \tag{8b}$$

where $\Delta T = T - T_0$ is the temperature variation from the reference temperature T_0 at which there is no thermal strain. Matrix *A* is defined as

$$\begin{bmatrix} A_x \\ A_y \\ A_{xy} \end{bmatrix} = -\begin{bmatrix} \bar{Q}_{11} & \bar{Q}_{12} & \bar{Q}_{16} \\ \bar{Q}_{12} & \bar{Q}_{22} & \bar{Q}_{26} \\ \bar{Q}_{16} & \bar{Q}_{26} & \bar{Q}_{66} \end{bmatrix} \begin{bmatrix} 1 & 0 \\ 0 & 1 \\ 0 & 0 \end{bmatrix} \begin{bmatrix} \alpha_{11} \\ \alpha_{22} \end{bmatrix} \tag{8c}$$

where α_{11} and α_{22} are the thermal expansion coefficients in the longitudinal and transverse directions, respectively. Substituting Eqs. (4)-(6) into Eq. (3) and considering Eqs. (7)-(8), a set of governing differential equations of motion is obtained as follows:

$$\begin{aligned} & \frac{\partial (N_m)_{xx}}{\partial x} + \frac{\partial N_x^T}{\partial x} + \frac{\partial (N_m)_{xy}}{\partial y} + \frac{\partial N_{xy}^T}{\partial y} \\ & = I_{0i}\frac{\partial^2 U_0}{\partial t^2} + \left(I_{1i} - \frac{4}{3h^2}I_{3i}\right)\frac{\partial^2 \psi_x}{\partial t^2} \\ & - \frac{4}{3h^2}I_{3i}\frac{\partial^2}{\partial t^2}\left(\frac{\partial W_0}{\partial x}\right) + q_x \end{aligned} \tag{9a}$$

$$\begin{aligned} & \frac{\partial (N_m)_{yy}}{\partial y} + \frac{\partial N_y^T}{\partial y} + \frac{\partial (N_m)_{xy}}{\partial x} + \frac{\partial N_{xy}^T}{\partial x} \\ & = I_{0i}\frac{\partial^2 V_0}{\partial t^2} + \left(I_{1i} - \frac{4}{3h^2}I_{3i}\right)\frac{\partial^2 \psi_y}{\partial t^2} \\ & - \frac{4}{3h^2}I_{3i}\frac{\partial^2}{\partial t^2}\left(\frac{\partial W_0}{\partial y}\right) + q_y \end{aligned} \tag{9b}$$

$$\begin{aligned}
&\frac{\partial}{\partial x}\Bigg[\frac{1}{2}\left((N_m)_{xx}+N_x^T\right)\frac{\partial W_0}{\partial x}-\frac{4}{3h^2}\left(P_{xx}+P_x^T\right)\frac{\partial W_0}{\partial x}+Q_x \\
&\quad-\frac{4}{h^2}R_x+\left((N_m)_{xy}+N_{xy}^T\right)\frac{\partial W_0}{\partial y} \\
&\quad-\frac{8}{3h^2}\left(P_{xy}+P_{xy}^T\right)\frac{\partial W_0}{\partial y}\Bigg] \\
&\quad+\frac{\partial}{\partial y}\Bigg[\frac{1}{2}\left((N_m)_{yy}+N_y^T\right)\frac{\partial W_0}{\partial y} \\
&\quad-\frac{4}{3h^2}\left(P_{yy}+P_y^T\right)\frac{\partial W_0}{\partial y}+Q_y-\frac{4}{h^2}R_y \\
&\quad+\left((N_m)_{xy}+N_{xy}^T\right)\frac{\partial W_0}{\partial x} \\
&\quad-\frac{8}{3h^2}\left(P_{xy}+P_{xy}^T\right)\frac{\partial W_0}{\partial x}\Bigg] \\
&\quad=P(x,y,t)-\left(K_1W_0-K_2\nabla^2W_0\right) \\
&\quad+I_{0i}\frac{\partial^2W_0}{\partial t^2} \\
&\quad-\frac{4}{3h^2}I_{3i}\left[\frac{\partial}{\partial x}\left(\frac{\partial^2U_0}{\partial t^2}\right)+\frac{\partial}{\partial y}\left(\frac{\partial^2V_0}{\partial t^2}\right)\right] \\
&\quad-\frac{4}{3h^2}I_{4i}\left[\frac{\partial}{\partial x}\left(\frac{\partial^2\psi_x}{\partial t^2}\right)+\frac{\partial}{\partial y}\left(\frac{\partial^2\psi_y}{\partial t^2}\right)\right] \\
&\quad-\frac{16}{9h^4}I_{6i}\left(\frac{\partial}{\partial x}\left(\frac{\partial^2\psi_x}{\partial t^2}+\frac{\partial^2 W_0}{\partial t^2}\right)\right. \\
&\quad\left.+\frac{\partial}{\partial y}\left(\frac{\partial^2\psi_y}{\partial t^2}+\frac{\partial^2 W_0}{\partial t^2}\right)\right)
\end{aligned} \tag{9c}$$

$$\begin{aligned}
&Q_x-\frac{4}{h^2}R_x+\frac{\partial}{\partial x}\left(S_{xx}+S_x^T\right)+\frac{\partial}{\partial y}\left(S_{xy}+S_{xy}^T\right) \\
&\quad=I_{1i}\frac{\partial^2U_0}{\partial t^2}+I_{2i}\frac{\partial^2\psi_x}{\partial t^2} \\
&\quad-\frac{4}{3h^2}I_{4i}\left[2\frac{\partial^2\psi_x}{\partial t^2}+\frac{\partial}{\partial x}\left(\frac{\partial^2 W_0}{\partial t^2}\right)\right] \\
&\quad+\frac{16}{9h^4}I_{6i}\left[\frac{\partial^2\psi_x}{\partial t^2}+\frac{\partial}{\partial x}\left(\frac{\partial^2 W_0}{\partial t^2}\right)\right]
\end{aligned} \tag{9d}$$

$$\begin{aligned}
&Q_y-\frac{4}{h^2}R_y+\frac{\partial}{\partial y}\left(S_{yy}+S_y^T\right)+\frac{\partial}{\partial x}\left(S_{xy}+S_{xy}^T\right) \\
&\quad=I_{1i}\frac{\partial^2V_0}{\partial t^2}+I_{2i}\frac{\partial^2\psi_y}{\partial t^2} \\
&\quad-\frac{4}{3h^2}I_{4i}\left[2\frac{\partial^2\psi_y}{\partial t^2}+\frac{\partial}{\partial y}\left(\frac{\partial^2 W_0}{\partial t^2}\right)\right] \\
&\quad+\frac{16}{9h^4}I_{6i}\left[\frac{\partial^2\psi_y}{\partial t^2}+\frac{\partial}{\partial y}\left(\frac{\partial^2 W_0}{\partial t^2}\right)\right]
\end{aligned} \tag{9e}$$

3. Solution Method

3.1 Nonlinear dynamic equations of plate frequency

To find the vibration frequencies of the sandwich plate considered in this study, Navier's solution is employed. Accounting for clamped boundary conditions, the displacement fields are defined as follows:

$$U_0=\sum_{\kappa=1}^{\infty}\sum_{\lambda=1}^{\infty}U_{\kappa\lambda}\sin\frac{2\pi x}{a}\left(1-\cos\frac{2\pi y}{b}\right)e^{-i\omega_{\kappa\lambda}t}, \tag{10a}$$

$$V_0=\sum_{\kappa=1}^{\infty}\sum_{\lambda=1}^{\infty}V_{\kappa\lambda}\left(1-\cos\frac{2\pi x}{a}\right)\sin\frac{2\pi y}{b}\,e^{-i\omega_{\kappa\lambda}t}, \tag{10b}$$

$$W_0=\sum_{\kappa=1}^{\infty}\sum_{\lambda=1}^{\infty}W_{\kappa\lambda}\left(1-\cos\frac{2\pi x}{a}\right)\left(1-\cos\frac{2\pi y}{b}\right)e^{-i\omega_{\kappa\lambda}t}, \tag{10c}$$

$$\Psi_x=\sum_{\kappa=1}^{\infty}\sum_{\lambda=1}^{\infty}\Psi_{x\kappa\lambda}\sin\frac{2\pi x}{a}\left(1-\cos\frac{2\pi y}{b}\right)e^{-i\omega_{\kappa\lambda}t}, \tag{10d}$$

$$\Psi_y=\sum_{\kappa=1}^{\infty}\sum_{\lambda=1}^{\infty}\Psi_{y\kappa\lambda}\left(1-\cos\frac{2\pi x}{a}\right)\sin\frac{2\pi y}{b}\,e^{-i\omega_{\kappa\lambda}t}, \tag{10e}$$

where $\omega_{\kappa\lambda}$ is the natural frequency of the sandwich plate, and κ, λ are the half-sine mode shapes. The method presented in this study can divide the thickness of the plate into the desired number of plies. It is helpful, especially in the case of having FGMs, to accurately predict the material properties, plate responses, and frequencies. Accordingly, three layers are considered along with FGM face sheets as seen in Fig. 2.

Substituting Eq. (10) into Eq. (9) results in Eq. (11) by which the frequencies of the sandwich plate can be calculated.

$$\begin{aligned}
&c_1U+c_2V+c_3W+c_4W^2+c_5\psi_x \\
&\quad+c_6\psi_y+c_7\ddot{U}+c_8\ddot{\psi}_x \\
&\quad+c_9\ddot{W}-c_{10}\Delta T_{xi}-c_{11}\Delta T_{yi} \\
&\quad-q_x=0
\end{aligned} \tag{11a}$$

$$\begin{aligned}
&d_1U+d_2V+d_3W+d_4W^2+d_5\psi_x \\
&\quad+d_6\psi_y+d_7\ddot{V}+d_8\ddot{\Psi}_y \\
&\quad+d_9\ddot{W}-d_{10}\Delta T_{yi} \\
&\quad-d_{11}\Delta T_{xi}-q_y=0
\end{aligned} \tag{11b}$$

$$\begin{aligned}
&e_1UW+e_2VW+e_3\psi_xW+e_4\psi_yW+e_5W \\
&\quad+e_6W^2+e_7W^3+e_8\psi_x \\
&\quad+e_9\psi_y-e_{10}\ddot{W}-e_{11}\ddot{U} \\
&\quad-e_{12}\ddot{V}-e_{13}\ddot{\psi}_x \\
&\quad-e_{14}\ddot{\psi}_y+e_{15}W\Delta T_{xi} \\
&\quad+e_{16}W\Delta T_{yi}-P(x,y,t) \\
&\quad+(K_1W_0-K_2\nabla^2W_0)=0
\end{aligned} \tag{11c}$$

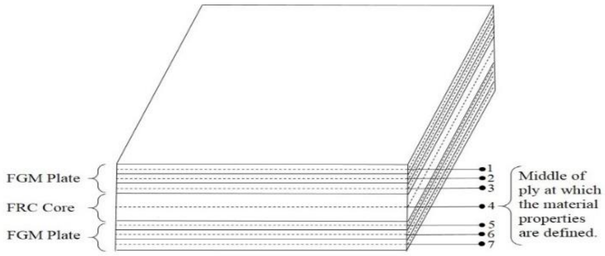

Fig. 2 Sandwich plate layout and ply midline for defining material properties

$$f_1U + f_2V + f_3W + f_4W^2 + f_5\psi_x + f_6\psi_y + f_7\ddot{U} + f_8\ddot{\psi}_x + f_9\ddot{W} + f_{10}\Delta T_{xi} + f_{11}\Delta T_{yi} = 0 \tag{11d}$$

$$g_1U + g_2V + g_3W + g_4W^2 + g_5\psi_x + g_6\psi_y + g_7\ddot{V} + g_8\ddot{\psi}_y + g_9\ddot{W} + g_{10}\Delta T_{yi} + g_{11}\Delta T_{xi} = 0 \tag{11e}$$

Coefficients of Eq. (11), c_i, d_i, e_i, f_i and g_i are given in Appendix A.

3.2 Natural frequency

To find the natural frequencies of the sandwich plate, the external forces should be set to zero. The general equation by which the free vibration of a system is calculated can be stated as given in Eq. (12) (Natarajan and Manickam 2012)

$$[K] - \omega_{\kappa\lambda}{}^2[M] = 0, \tag{12}$$

where *[K]* is the stiffness matrix, $[M\ ]$ is the mass matrix and $\omega_{\kappa\lambda}$ is the natural frequency. The set of equations of natural frequencies of a sandwich plate can be stated in the form of a matrix, with respect to Eq. (12), as

$$([\chi]_{5\times16} - \omega_{\kappa\lambda}{}^2[M]_{5\times16})\begin{pmatrix} U \\ V \\ W \\ W^2 \\ \psi_x \\ \psi_y \\ \ddot{U} \\ \ddot{V} \\ \ddot{W} \\ \ddot{\psi}_x \\ \ddot{\psi}_y \\ UW \\ VW \\ \psi_xW \\ \psi_yW \\ W^3 \end{pmatrix}_{16\times1} = 0, \tag{13}$$

where $[\chi]$ is the coefficient matrix, $[M]$ the mass matrix, and ω the natural frequency of the sandwich plate. The elements of matrices $[\chi]$ and $[M]$ are provided in Appendices B and C, respectively.

3.3 Evaluation of the validity of the suggested method

To verify the validity of the method presented in this study, the non-dimensional fundamental frequencies of the sandwich plate with FGM face sheets are calculated and compared with the results reported by (Li *et al.* 2009, Wang and Shen 2011*)*. The material properties of the FGM face sheets are $E_c = 380\text{GPa}$, $\rho_c = 3800\,{}^{kg}/_{m^3}$ for alumina (Al_2O_3), one of the most cost effective and widely used materials in engineering ceramics, which is used for the top surface of FGM sheets or ceramic parts and $E_m = 70\text{GPa}$, $\rho_m = 2707\,{}^{kg}/_{m^3}$ for aluminum which is considered for the bottom face of an FGM sheet and a core as well. The Poisson's ratio for the core (υ_c) and the face sheet (υ_F) are assumed to be constant, since the effect of Poisson's ratio on the sandwich plate responses is much less than that of the elastic modulus, and equal to each other: $\upsilon_F = \upsilon_c = 0.3$. The non-dimensional natural frequency parameter is defined as Eq. (14) presents (Gholami and Ansari 2018):

$$\widetilde{\omega} = \omega\left(\frac{c^2}{h}\right)\sqrt{{}^{\rho_0}/_{E_0}} \tag{14}$$

where $\rho_0 = 1\,{}^{kg}/_{m^3}$ and $E_0 = 1\text{GPa}$.

The effective material properties (P_F), such as elastic modulus E_f, density ρ_F, Poisson's ratio υ_f, and thermal expansion coefficient, α_f are defined as given in Eq. (15) (Mohammadzadeh and Noh 2017):

$$P_F = P_cV_c + P_mV_m, \tag{15}$$

where P_c and P_m denote the temperature-dependent properties of the ceramic and metal, respectively. Here, V_c is the volume fraction of ceramic, while V_m is the volume fraction of the metal as described in Eq. (16) (Wang *et al.* 2017):

$$V_{mt} = \left(\frac{Z-t_0}{t_1-t_0}\right)^N,\ V_{mb} = \left(\frac{t_3-Z}{t_3-t_2}\right)^N,\ V_m + V_c = 1, \tag{16}$$

where N is the volume fraction index, which dictates the material variation profile through the FGM layer thickness, and indices *t* and *b* represent the top and bottom faces of layers, respectively.

The core to face sheet thickness ratio is $\frac{h_C}{h_F}$ =8. Various volume fraction index values (N) of 0.0, 0.5, 1.0, 5.0, and 10.0 are considered, so the material properties shall be defined with respect to N. To consider gradual variation of material properties through the thickness of an FGM sheet, each face sheet is divided into three layers, top, middle, and bottom, as seen in Fig. 2. The material properties of the FGM face sheets are provided in Table 1.

The material properties given in Table 1 together with Eq. (13) are employed to find the natural frequencies of a sandwich plate. For this aim, the Runge–Kutta method, as well as MAPLE 14, are used. Thereafter, Eq. (14) is used to calculate the non-dimensional natural frequencies of a sandwich plate. Table 2 shows a comparison of the results

Table 1 Material properties of FGM faces with respect to the variation of N

Layer position	N	E_F(GPa)	$\rho_F \, {kg}/{m^3}$	$\alpha_F * {10^{-6}}/{C^{\circ}}$	ν_F
Top	0.00	70.00	2707.00	23.10	0.30
Top	0.50	253.44	3353.78	13.69	0.30
Top	1.00	328.33	3617.83	9.85	0.30
Top	5.00	379.96	3799.86	7.20	0.30
Top	10.00	380.00	3800.00	7.20	0.30
Middle	0.00	70.00	2707.00	23.10	0.30
Middle	0.50	160.80	3027.13	18.44	0.30
Middle	1.00	225.00	3253.50	15.15	0.30
Middle	5.00	370.31	3765.84	7.70	0.30
Middle	10.00	379.70	3798.93	7.22	0.30
Bottom	0.00	70.00	2707.00	23.10	0.30
Bottom	0.50	97.01	2802.23	21.71	0.30
Bottom	1.00	121.67	2889.17	20.45	0.30
Bottom	5.00	255.42	3360.75	13.59	0.30
Bottom	10.00	329.93	3623.47	9.77	0.30

Table 2 Non-dimensional natural frequencies $\tilde{\omega}$

b/h	Source	N 0.0	0.5	1.0	5.0	10.0
100	Li *et al.* (2009)	0.96022	1.26557	1.38331	1.57035	1.60457
100	Wang & *Shen 2011*	0.96022	1.26557	1.38332	1.57036	1.60458
100	Present (Analytical)	0.96015	1.26468	1.38314	1.57028	1.60445
100	Present (ABAQUS)	0.96007	1.26270	1.38119	1.57016	1.60327
Error (%)	Li & present	0.00700	0.07000	0.01200	0.00400	0.00700
Error (%)	Wang & present	0.00700	0.07000	0.01300	0.00500	0.00800
10	Li *et al.* (2009)	0.92897	1.20553	1.30825	1.46647	1.49481
10	Wang & *Shen 2011*	0.92839	1.20559	1.30854	1.46696	1.49535
10	Present (Analytical)	0.92813	1.20535	1.30803	1.46597	1.49458
10	Present (ABAQUS)	0.92705	1.20349	1.30472	1.46382	1.49228
Error (%)	Li & present	0.09000	0.01500	0.01700	0.03400	0.01500
Error (%)	Wang & present	0.02800	0.02000	0.03900	0.06700	0.05100

of this study with those reported in the literature. The differences among the results obtained from the analytical method of this study and those of the literature are calculated and reported in Table 2 as Error (%).

As seen in Table 2, the non-dimensional natural frequencies obtained from the present study, which were obtained by analytical and numerical methods, and those of (Li *et al.* 2009, Wang and Shen 2011*)* show good agreement.

The system of nonlinear dynamic equations cannot be directly solved and lead to an exact solution, so the Runge–Kutta scheme is employed. To provide an explanation of the error, it is only possible to estimate the error. For this aim, the one-step method can be used as follows.

Table 3 Calculation of the error of Runge Kutta Method

Step size	Error
0.002	0.08123
0.001	0.03253
0.0005	0.00654
0.00025	0.00125
0.000125	0.00009
0.0000625	0.00002

The one-step method is a 5th-order Runge–Kutta formula which is embedded in a 4th-order Runge–Kutta formula as follows as Eq. (17) presents (Mohammadzadeh and Noh 2017):

$$\begin{aligned}
&k_0 = hf(x_n, y_n),\\
&k_1 = hf(x_n + {h}/{2}, y_n + {k_0}/{2}),\\
&k_2 = hf(x_n + h, y_n + {(k_0 + k_1}/{4}),\\
&k_3 = hf(x_n + h, y_n - k_1 + 2k_2),\\
&k_4 = hf(x_n + \tfrac{2h}{3}, y_n + \tfrac{(7k_0+10k_1+k_3)}{27}),\\
&k_5 = hf(x_n + \tfrac{2h}{10}, y_n + \tfrac{(28k_0-125k_1+546k_2+54k_3-378k_4)}{625})
\end{aligned} \tag{17a}$$

The fourth-order formula is expressed as

$$y_{n+1} = y_n + (k_0 + 4k_2 + k_3)/6 \tag{17b}$$

and the fifth-order formula is expressed as

$$y_{n+1} = y_n + (14k_0 + 35k_3 + 162k_4 + 125k_5)/336 \tag{17c}$$

Therefore, the error can be obtained by subtracting solutions obtained from both 4th-and 5th-order Runge-Kutta methods as follows:

$$E_{n+1} = (y_{n+1})_{4th} - (y_{n+1})_{5th} \tag{17d}$$

Considering the explanations above, the amounts of error are given in Table 3.

As seen in Table 3, the error is proportional to h^5, which agrees with the theory of the Runge- Kutta method.

3.3.1 Evaluation of convergence of the plate frequencies

Although the method was validated in the previous section, to have more reliable results, a convergence study was performed considering frequencies corresponding to five first mode shapes of the plate. To investigate the convergence of the sandwich plate frequencies, the numerical method was employed. For this aim, the example problem defined in method validity was used. The material properties given in Table 1 were specified to the sandwich plate corresponding to various values of volume fraction index, N = 0, 1.0, and 10. Fig. 3 presents the convergence of sandwich plate frequency with respect to mode shape.

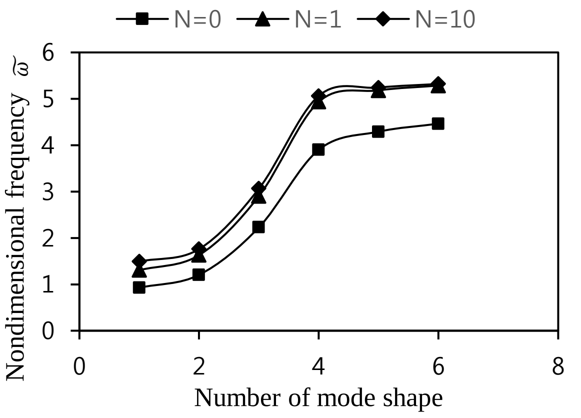

b/h=10

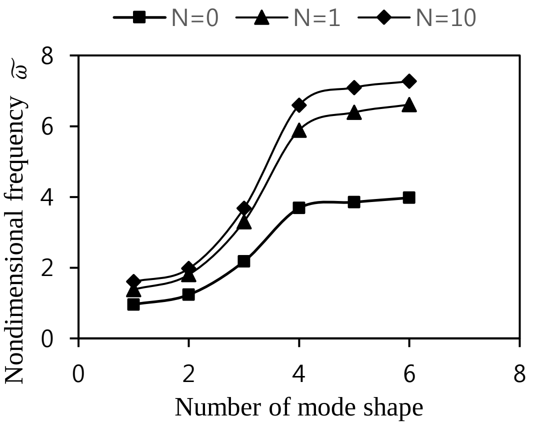

b/h=100

Fig. 3 Convergence of sandwich plate frequency for various volume fraction index (N) values with respect to mode shape

As seen in Fig. 3, convergence was obtained for the sandwich plate frequencies, and after mode 4, the increase in plate frequency is negligible. Therefore, the results are reliable, and the method can be used for further study and nonlinear dynamic analyses.

3.4 Effects of temperature change and volume fraction index

In this part, an attempt is made to investigate the effects of the temperature change and volume fraction index N on the frequencies of a sandwich plate having 3 layers, FGM/FRC/FGM, resting on elastic foundations. The core-to-face sheet thickness ratio of $h_C/h_F = 10$ is considered, while the aspect ratio of *a/c*=1 is specified to the plate. A range of volume fraction index, N, from 0 to 10 as well as three different temperatures of T =300 K (27 ℃), 500 K (227 ℃) and 700 K (427 ℃) for which the material properties of FGM face sheets with respect to various amounts of volume fraction index, N, are provided in Tables 4–6, respectively. Since high temperatures occur in burst events, fires, and nuclear explosions, the high temperatures of 500 K and 700 K are taken into account in this study.

The provided material properties are specified to the face sheets of the sandwich plate to calculate the natural

Table 4 Material properties of FGM faces for various N (T= 300K, 27℃)

Layer position	N	E_F(GPa)	$\rho_F\ {kg}/{m^3}$	$\alpha_F * {10^{-6}}/{C^\circ}$	ν_F
Top	0	105.70	2707.00	6.94	0.29
Top	0.5	142.60	3353.78	13.83	0.29
Top	1	157.67	3617.83	16.65	0.29
Top	5	168.05	3799.86	18.59	0.29
Top	10	168.06	3800.00	18.59	0.29
Middle	0	105.70	2707.00	6.94	0.29
Middle	0.5	123.96	3027.13	10.35	0.29
Middle	1	136.88	3253.50	12.77	0.29
Middle	5	166.11	3765.84	18.23	0.29
Middle	10	168.00	3798.93	18.58	0.29
Bottom	0	105.70	2707.00	6.94	0.29
Bottom	0.5	111.13	2802.23	7.96	0.29
Bottom	1	116.09	2889.17	8.88	0.29
Bottom	5	143.00	3360.75	13.91	0.29
Bottom	10	157.99	3623.47	16.71	0.29

Table 5 Material properties of FGM faces for various N (T= 500K, 227℃)

Layer position	N	E_F(GPa)	$\rho_F\ {kg}/{m^3}$	$\alpha_F * {10^{-6}}/{C^\circ}$	ν_F
Top	0	94.46	2707.00	4.13	0.29
Top	0.5	121.24	3353.78	22.54	0.29
Top	1	132.18	3617.83	30.06	0.29
Top	5	139.71	3799.86	35.24	0.29
Top	10	139.72	3800.00	35.25	0.29
Middle	0	94.46	2707.00	4.13	0.29
Middle	0.5	107.71	3027.13	13.25	0.29
Middle	1	117.09	3253.50	19.69	0.29
Middle	5	138.30	3765.84	34.27	0.29
Middle	10	139.68	3798.93	35.22	0.29
Bottom	0	94.46	2707.00	4.13	0.29
Bottom	0.5	98.40	2802.23	6.84	0.29
Bottom	1	102.00	2889.17	9.32	0.29
Bottom	5	121.53	3360.75	22.74	0.29
Bottom	10	132.41	3623.47	30.22	0.29

frequencies of the sandwich plate for the corresponding volume fraction index and temperature. The obtained frequencies are normalized by employing Eq. (14) and reported as non-dimensional natural frequencies as given in Table 7.

As seen in Table 7, with increasing temperature, the natural frequencies of the plate decrease. This can be seen for all values of T and N. The reason is that increasing temperature leads to a decrease in sandwich plate stiffness since only the elastic modulus is decreased as temperature increases, so natural frequencies are decreased. The investigation into the effects of N on non-dimensional

Table 6 Material properties of FGM faces for various N (T= 700K, 427℃)

Layer position	N	E_F(GPa	$\rho_F\ {}^{kg}/_{m^3}$	$\alpha_F * {}^{10^{-6}}/_{C^\circ}$	ν_F
Top	0.0	83.22	2707.00	-0.59	0.29
Top	0.5	107.53	3353.78	36.49	0.29
Top	1.0	117.46	3617.83	51.63	0.29
Top	5.0	124.30	3799.86	62.07	0.29
Top	10.0	124.31	3800.00	62.07	0.29
Middle	0.0	83.22	2707.00	-0.59	0.29
Middle	0.5	95.25	3027.13	17.77	0.29
Middle	1.0	103.76	3253.50	30.74	0.29
Middle	5.0	123.03	3765.84	60.12	0.29
Middle	10.0	124.27	3798.93	62.01	0.29
Bottom	0.0	83.22	2707.00	-0.59	0.29
Bottom	0.5	86.80	2802.23	4.87	0.29
Bottom	1.0	90.06	2889.17	9.86	0.29
Bottom	5.0	107.79	3360.75	36.89	0.29
Bottom	10.0	117.67	3623.47	51.95	0.29

Table 7 Non-dimensional natural frequencies obtained from analytical approach considering variation of N and T (a/c= 1, c/h= 100)

No	Temperature(K)	N	$\tilde{\omega}$
1		0.0	0.9865
2		0.5	0.9894
3	300	1.0	0.9906
4		5.0	0.9921
5		10.0	0.9924
6		0.0	0.9783
7		0.5	0.9777
8	500	1.0	0.9770
9		5.0	0.9753
10		10.0	0.9749
11		0.0	0.9698
12		0.5	0.9686
13	700	1.0	0.9678
14		5.0	0.9655
15		10.0	0.9648

natural frequencies $\tilde{\omega}$ shows that for the temperature of 300 K, increasing N results in increasing $\tilde{\omega}$. It occurs because N directly affects the face sheet stiffness, so the natural frequency increases. For the higher temperatures of 500 K and 700 K, a reverse trend was observed, as shown in Fig. 4.

As seen in Fig. 4, non-dimensional frequencies $\tilde{\omega}$, vary differently with respect to the volume fraction index N, for different temperatures. For the temperature of 300 K, as the volume fraction index increases, the plate frequency increases. It should be noted that for N<1, changes in frequencies are larger than those for N>1. A steep slope is observed in the graph for N<1. The graph corresponding

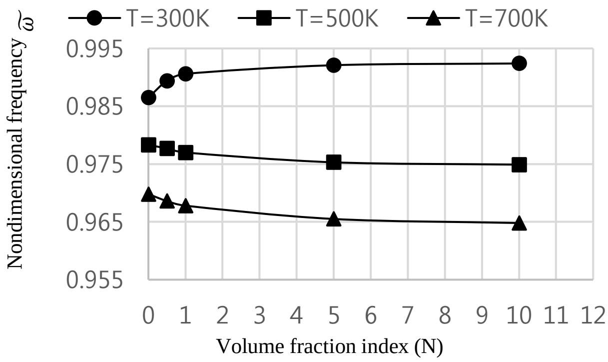

Fig. 4 Variation of the non-dimensional frequency with respect to N

to 300 K plateaus after N=3. The graphs corresponding to 500 K and 700 K are descending; the plate frequencies decrease as the volume fraction index increases. For 500 K and for N<2 a steep slope can be seen which shows a sudden drop in natural frequencies, and the graph plateaus for N>4. For the graph corresponding to 700 K, a steep slope is seen for N<3, and the graph plateaus when N>5. From these results, it can be inferred that as the temperature increases, the plate frequencies decrease. This phenomenon can be described based on Eq. (18), which relates the elastic modulus of the materials to the temperature and volume fraction index (Mohammadzadeh and Noh 2017):

$$E_F(Z,T) = \left(E_b(T) - E_t(T)\right)\left(\frac{2Z+h}{2h}\right)^N + E_t, \tag{18}$$

where $E_F(Z,T)$ is the elastic modulus of the plate materials as a function of temperature, depth in thickness and N, $E_b(T)$ temperature-dependent elastic modulus at the bottom of face sheet and $E_t(T)$ temperature-dependent elastic modulus at the top of the face sheet. In the case of this study, for the temperatures of 500 K and 700 K the numerical value of $\left(E_b(T) - E_t(T)\right)$ is negative (refer to Tables 5 and 6), and increasing N results in a larger value of $\left(\frac{2Z+h}{2h}\right)^N$, so a larger amount is subtracted from E_t. Therefore, a smaller amount is obtained for E_F, which means that the stiffness of the face sheets is decreased, and it leads to smaller $\tilde{\omega}$. Figs. 5–7 present the variation of the non-dimensional fundamental natural frequencies of a sandwich plate having FGM face sheets with respect to side-to-thickness ratio, c/h, considering various volume fraction index values and for various temperatures of 300 K, 500 K, and 700 K, respectively.

The results shown in Figs. 5–7 indicate that increasing temperature leads to lower natural frequencies. A reason for this phenomenon is that the FGM characteristics are temperature dependent; that is, the material properties of the face sheets vary as the temperature changes. Increasing temperature results in decreased sandwich plate face sheet stiffness, so considering Eq. (12), the natural frequencies of the sandwich plate decrease.

Investigation into the variation of the natural frequency of the sandwich plate with respect to change in values of *c/h* shows that by increasing the side-to-thickness ratio in the

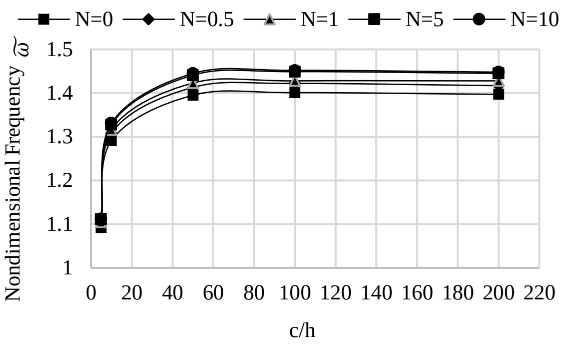

Fig. 5 Non-dimensional fundamental natural frequencies versus c/h considering various N for 300K

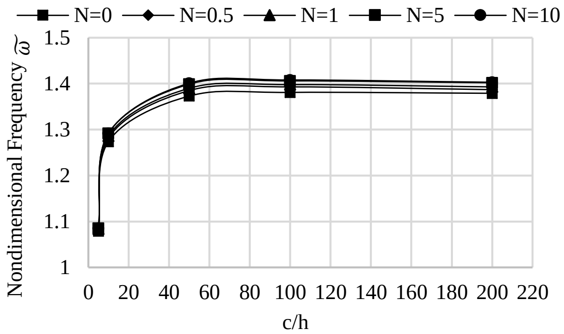

Fig. 6 Non-dimensional fundamental natural frequencies versus c/h considering various N for 500K

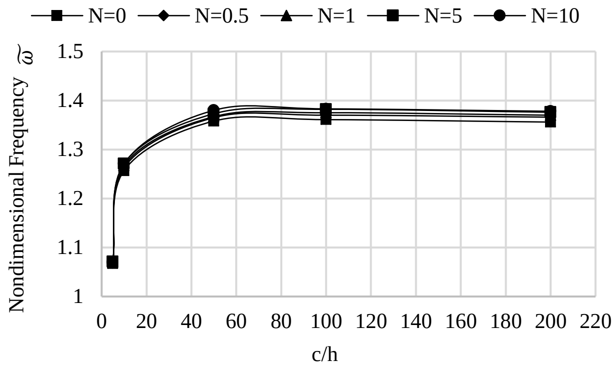

Fig. 7 Non-dimensional fundamental natural frequencies versus c/h considering various N for 700K

range *1<c/h<60* which can be categorized as a batch of thick plates, a non-linear sudden increase in the non-dimensional natural frequency of the sandwich plate $\widetilde{\omega}$ can be observed as shown in Figs. 5–7. Moreover, the effects of an increase in *c/h* on $\widetilde{\omega}$ for the range of *c/h>60,* which can be indicated as thin plates, is infinitesimal and can be neglected.

3.5 Nonlinear vibration

The nonlinear vibrations of a sandwich plate are calculated and presented in Table 8 in the form of nonlinear-to-linear frequency ratios for *c/h=1*, and considering the effects of foundation stiffness, various temperatures, and volume fraction index N. The nonlinearity is considered as effects of existent initial displacement in the form of the ratio of maximum central displacement to the plate thickness, $\frac{W_{max}}{h}$. The results given in Table 8 show that the natural frequencies of the sandwich plate decrease with increasing temperature for the same volume fractions, while they increase with increases in the volume fraction index N and the foundation stiffness. In contrast, the nonlinear-to-linear frequency ratios are reduced with an increase in the foundation stiffness for the same volume fractions, and the temperature change has a very small effect on the nonlinear-to-linear frequency ratios of the same plate and the same volume fractions.

Table 8-1 Nonlinear frequencies of the sandwich plate in the form of $\omega_{NL}/_{L}$ for various N and $\frac{W_{max}}{h} < 1.0$

(K1, K2)	Temperature(K)	N	$\widetilde{\omega}$	W_{max}/h 0.1	0.25	0.5	0.75
(0, 0)	300	0.0	0.9865	1.0135	1.0513	1.1432	1.2562
		1.0	0.9906	1.0088	1.0476	1.1341	1.2413
		5.0	0.9921	1.0026	1.0368	1.1295	1.2314
	500	0.0	0.9783	1.0102	1.0513	1.1432	1.2562
		1.0	0.9770	1.0088	1.0463	1.1364	1.2413
		5.0	0.9753	1.0056	1.0427	1.1296	1.2239
	700	0.0	0.9698	1.0102	1.0513	1.1432	1.2562
		1.0	0.9678	1.0089	1.0471	1.1409	1.2499
		5.0	0.9655	1.0029	1.0357	1.1329	1.2339
(10, 0)	300	0.0	1.1147	1.0092	1.0351	1.1071	1.1963
		1.0	1.2116	1.0051	1.0345	1.1064	1.1948
		5.0	1.6222	1.0018	1.0328	1.1025	1.1917
	500	0.0	1.0667	1.0085	1.0346	1.1032	1.1892
		1.0	1.1844	1.0081	1.0328	1.0278	1.1786
		5.0	1.4747	1.0073	1.0309	1.0246	1.1705
	700	0.0	1.0217	1.0080	1.0325	1.0988	1.1826
		1.0	1.1123	1.0075	1.0304	1.0955	1.1776
		5.0	1.4045	1.0066	1.0273	1.0933	1.1746
(10, 1)	300	0.0	1.3376	1.0042	1.0178	1.0697	1.1558
		1.0	1.4152	1.0040	1.0165	1.0676	1.1521
		5.0	1.4548	1.0038	1.0157	1.0667	1.1514
	500	0.0	1.2986	1.0036	1.0157	1.0622	1.1477
		1.0	1.3572	1.0035	1.0151	1.0590	1.1455
		5.0	1.3952	1.0034	1.0148	1.0586	1.1446
	700	0.0	1.2583	1.0031	1.0136	1.0569	1.1386
		1.0	1.3151	1.0030	1.0131	1.0563	1.1371
		5.0	1.3545	1.0028	1.0129	1.0556	1.1362

3.5.1 Backbone curve

The main idea of backbone curves is that, for most structures, resonances lead to the largest vibration amplitude, so the resonant responses must be understood. This is relatively straightforward for a linear system because resonances occur independently of each other and

Table 8-2 Nonlinear frequencies of the sandwich plate in the form of $\omega_{NL}/_{L}$ for various N and $1.0 \leq \frac{W_{max}}{h} \leq 2.0$

(K1, K2)	Temperature(K)	N	$\tilde{\omega}$	W_{max}/h 1.0	1.25	1.5	1.75	2.0
(0, 0)	300	0.0	0.9865	1.3858	1.5330	1.7049	1.9033	2.1362
		1.0	0.9906	1.3632	1.5025	1.6649	1.8488	2.0620
		5.0	0.9921	1.3449	1.4730	1.6189	1.7847	1.9743
	500	0.0	0.9783	1.3832	1.5275	1.6988	1.8965	2.1286
		1.0	0.9770	1.3611	1.4965	1.6497	1.8239	2.0239
		5.0	0.9753	1.3294	1.4481	1.5802	1.7291	1.8991
	700	0.0	0.9698	1.3846	1.5307	1.7043	1.9047	2.1343
		1.0	0.9678	1.3679	1.5010	1.6527	1.8234	2.0217
		5.0	0.9655	1.3242	1.4385	1.5684	1.7148	1.8811
(10, 0)	300	0.0	1.1147	1.2971	1.4128	1.5444	1.6980	1.8872
		1.0	1.2116	1.2944	1.4087	1.5394	1.6923	1.8676
		5.0	1.6222	1.2902	1.4048	1.5331	1.6812	1.8514
	500	0.0	1.0667	1.2851	1.3985	1.5288	1.6751	1.8478
		1.0	1.1844	1.3522	1.5527	1.7875	2.0613	2.3816
		5.0	1.4747	1.3393	1.5338	1.7597	2.0212	2.3245
	700	0.0	1.0217	1.2762	1.3829	1.5024	1.6370	1.7902
		1.0	1.1123	1.2913	1.4197	1.5650	1.7303	1.9200
		5.0	1.4045	1.2759	1.3898	1.5166	1.6594	1.8226
(10, 1)	300	0.0	1.3376	1.2533	1.3641	1.4897	1.6367	1.8116
		1.0	1.4152	1.2496	1.3618	1.4904	1.6379	1.8110
		5.0	1.4548	1.2506	1.3646	1.4997	1.6533	1.8334
	500	0.0	1.2986	1.2432	1.3534	1.4771	1.6168	1.7821
		1.0	1.3572	1.2451	1.3590	1.4900	1.6385	1.8061
		5.0	1.3952	1.2414	1.3508	1.4755	1.6186	1.7823
	700	0.0	1.2583	1.2299	1.3341	1.4536	1.5892	1.7423
		1.0	1.3151	1.2274	1.3308	1.4498	1.5853	1.7465
		5.0	1.3545	1.2265	1.3282	1.4430	1.5735	1.7237

respond only to external sources of excitation. However, for nonlinear systems, there is the possibility that resonances or modes can interact due to nonlinear coupling between different parts of the structure. Backbone curves can be used to help understand the complexities of resonant behavior. This is because the resonant response of a forced system is closely linked to the unforced response, and a backbone curve represents the unforced, undamped response.

To provide a better understanding of the nonlinear behavior of the sandwich plate, the backbone curves are provided in Fig. 8. The abscissa is specified to the ratio of the nonlinear vibration to the linear vibration, $\omega_{NL}/_{L}$, and the ordinate is specified to the maximum displacement to the plate thickness, $\frac{W_{max}}{h}$. They are derived for the various values of the volume fraction index, N, temperature, and foundation conditions.

As seen from the backbone curves in Fig. 8, by increasing the initial imperfection, the nonlinear vibration of the sandwich plate increases. This shows that resonance, in nonlinear vibration, is a function of imperfection. The volume fraction index, N, also has a significant effect on the nonlinear vibration of the sandwich plate for a large imperfection, $W_{max}/_{h}$, and Winkler foundation, K_1 = 10 and K_2 = 0. For the foundation conditions of K_1 = 10 and K_2=1, the volume fraction index has no significant effect on the nonlinear vibration of the system. From the graphs, it can be inferred that the nonlinear vibration of the sandwich plate is not a function of temperature.

4. Concluding Remarks

This study was motivated to provide a comprehensive nonlinear dynamic method for the investigation of one of the frequently used plated structures called sandwich plates. The most important dynamic parameter which should be highly paid attention is the vibration of a structure or structural component as it may lead to structural failure. In this regard, this study presented an analytical approach to investigate the frequencies of a sandwich plate with FGM face sheets. The interaction between the sandwich plate and the elastic foundation was taken into account as well as the effects of temperature variation which directly affects the material properties and consequently the stiffness of the plate. For the derivation of governing equations of motion of this study, the higher-order shear deformation theory was employed in conjunction with Hamilton's principle. The sinusoidal displacement fields satisfying the clamped boundary conditions were employed to convert the set of equation of motions to the solvable form of the set of nonlinear dynamic equations. The Runge-Kutta method was taken into account for solving the equations and finding the natural frequency and nonlinear frequency of the several cases of sandwich plates corresponding to various conditions. In order to evaluate the validity of the method, the results obtained from the method of this study were compared with those reported in the literature for some special cases. The results showed that as the temperature increased, the sandwich plate frequency decreased, as increasing temperature led to a decrease in the stiffness of the sandwich plate stiffness. For the temperature of 300 K, an increase in the volume fraction index, *N*, caused the non-dimensional natural frequencies, $\widetilde{\omega}$, to grow as *N* directly affects the face sheet stiffness. For the higher temperatures of 500 K and 700 K, a reverse trend was observed. A possible explanation is that an increase in *N* resulted in an increasing portion of mthe etal in the FGM face sheets for which the stiffness decreases with increase in temperature, so the natural frequencies decrease. Nonlinear vibration analyses of the sandwich plate were performed with consideration of the effects of foundation stiffness, temperature change, and *N*. For this aim, the geometrical nonlinearities were considered by imposing the initial displacement of different amounts to the plate in form of the ratio of displacement of the plate center to the plate thickness. The nonlinear frequencies were reported in the form of ra atio of the nonlinear frequency to the linear frequency or natural frequency of the desired case, $\omega_{NL}/_{L}$.

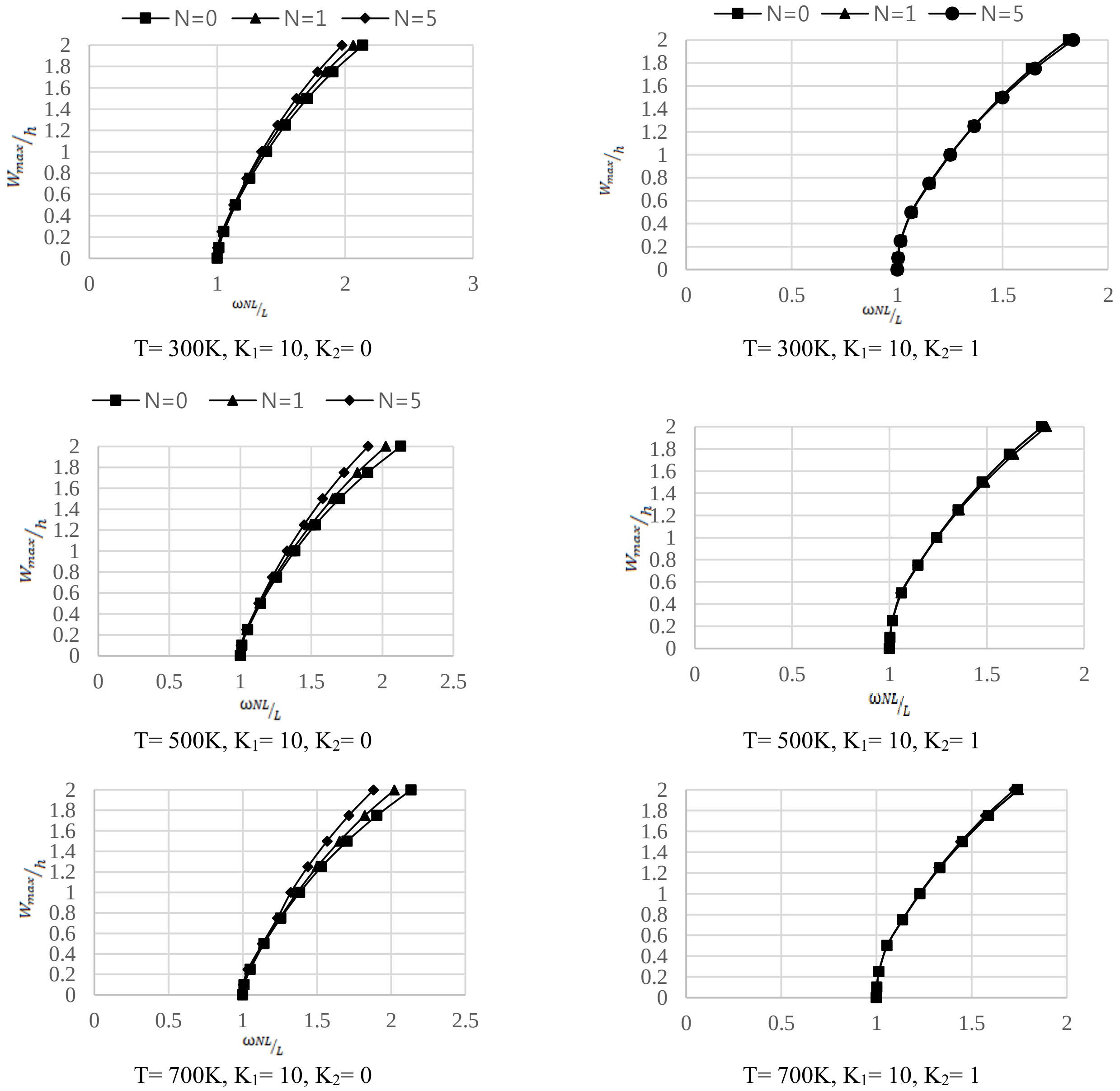

T= 300K, K_1= 10, K_2= 0

T= 300K, K_1= 10, K_2= 1

T= 500K, K_1= 10, K_2= 0

T= 500K, K_1= 10, K_2= 1

T= 700K, K_1= 10, K_2= 0

T= 700K, K_1= 10, K_2= 1

Fig. 8 Backbone curves of sandwich plates for various temperatures and foundation conditions

Results showed that the nonlinear-to-linear frequency ratios, $\omega_{NL}/_{L}$, decreased with an increase in the foundation stiffness. Temperature change had a very small effect on the nonlinear-to-linear frequency ratios of the same plate. For a better understanding of the nonlinear behavior of the sandwich plate the backbone curves were presented. It was observed that the nonlinear vibration of the plate did not depend on temperature change. Besides, *N* affected the nonlinear vibration of the plate only for the foundation conditions of K1 = 10 and K2 = 1. Further studies are required to investigate sandwich plate and composite plate frequencies in the case of severe loadings, such as blast loads which are accompanied by elevated temperature.

Acknowledgment

This research was supported by the Basic Science Research Program through the National Research Foundation of Korea (NRF) funded by the Ministry of Education, Science and Technology (Project No. 2015-041523).

References

Ahmadi, I. (2018), “Three-dimensional and free-edge hygrothermal stresses in general long sandwich plates”, *Struct. Eng. Mech.*, **65**(3), 275-290.

Alibeigloo, A. (2017), “Three dimensional coupled thermoelasticity solution of sandwich plate with FGM core under thermal shock”, *Compos. Struct.*, **177**, 96-103. https://doi.org/10.1016/j.compstruct.2017.06.046.

Arunkumar, M.P., Pitchaimani, J. and Gangadharan, KV. (2018), “Bending and free vibration analysis of foam-filled truss core sandwich panel”, *J. Sandwich Struct. Mater.*, **20**(5), 617-638. https://doi.org/10.1177/1099636216670612.

Belarbi, M.O., Tati, A., Ounis, H. and Benchabane, A. (2016), "Development of a 2D isoparametric finite element model based on the layerwise approach for the bending analysis of sandwich plates", *Struct. Eng. Mech.*, **57**(3), 473-506. https://doi.org/10.1007/s11029-019-09807-y.

Bouderba, B., Houari, M.S.A., Tounsi, A. and Mahmoud, S.R. (2016), "Thermal stability of functionally graded sandwich plates using a simple shear deformation theory", *Struct. Eng. Mech.*, **58**(3), 397-422. https://doi.org/10.12989/sem.2016.58.3.397.

Cadou, J.M., Boumediene, F., Guevel, Y., Girault, G., Duigou, L., Daya, E.M. and Potier-Ferry, M. (2016), "A high order reduction–correction method for Hopf bifurcation in fluids and for viscoelastic vibration", *Comput. Mech.*, **57**(2), 305-324. https://doi.org/10.1007/s00466-015-1232-4.

Choi, E., Mohammadzadeh, B., Kim, D. and Jeon, J.S. (2018), "A new experimental investigation into the effects of reinforcing mortar beams with superelastic SMA fibers on controlling and closing cracks", *Compos. Part B*, **137**, 140-152. https://doi.org/10.1016/j.compositesb.2017.11.017.

Choi, E., Chae, S.W., Park, H., Nam, T.H., Mohammadzadeh, B. and Hwang, J.H. (2018), "Investigating self-centering capacity of superelastic shape memory alloy fibers with different anchorages through pullout tests", *J. Nanosci. Nanotechnol.*, **18,** 6228-6232. https://doi.org/10.1166/jnn.2018.15635.

Choi, E., Mohammadzadeh, B., Hwang, J.H and Kim, W.J. (2018), "Pullout behavior of superelastic SMA fibers with various end-shapes embedded in cement mortar", *Construct. Build Mater.*, **167**, 605-616. https://doi.org/10.1016/j.conbuildmat.2018.02.070.

Daouadji, T.H. and Adim, B. (2017), "Mechanical behaviour of FGM sandwich plates using a quasi-3D higher order shear and normal deformation theory," *Struct. Eng. Mech.*, **61**(1), 49-63. https://doi.org/10.12989/sem.2017.61.1.049.

Demasi, L. (2013), "Partially layer wise advanced Zig Zag and HSDT models based on the generalized unified formulation", *Eng. Struct.,* **53**, 63-91. https://doi.org/10.1016/j.engstruct.2013.01.021.

Ebrahimi, F. and Heidari, E. (2018), "Vibration characteristics of advanced nanoplates in humid-thermal environment incorporating surface elasticity effects via differential quadrature method", *Struct. Eng. Mech.*, **68**(1), 131-157.

Elmossouess, B., Kebdani, S., Bouiadjra, M.B. and Tounsi, A. (2017), "A novel and simple HSDT for thermal buckling response of functionally graded sandwich plates", *Struct. Eng. Mech.*, **62**(4), 401-415. https://doi.org/10.12989/sem.2017.62.4.401.

El Meiche, N., Tounsi, A., Ziane, N., Mechab, I. and Adda.Bedia, E.A. (2011), "A new hyperbolic shear deformation theory for buckling and vibration of functionally graded sandwich plate", *J. Mech. Sci.*, **53**, 237-247. https://doi.org/10.1016/j.ijmecsci.2011.01.004.

Farokhi, H. and Ghayesh, M.H. (2015), "Nonlinear dynamical behaviour of geometrically imperfect microplates based on modified couple stress theory", *J. Mech. Sci.*, **90**, 133-144. https://doi.org/10.1016/j.ijmecsci.2014.11.002.

Farokhi, H., Ghayesh, M.H. and Ambili, M. (2013), "Nonlinear dynamics of a geometrically imperfect microbeam based on the modified couple stress theory", *J. Eng. Sci.*, **68**, 11-23. https://doi.org/10.1016/j.ijengsci.2013.03.001.

Farokhi, H. and Ghayesh, M.H. (2015), "Thermo-mechanical dynamics of perfect and imperfect Timoshenko microbeams", *J. Eng. Sci.*, **91**, 12-33. https://doi.org/10.1016/j.ijengsci.2015.02.005.

Farokhi, H., Ghayesh, M.H., Gholipour, A. and Hussain, S. (2017), "Motion characteristics of bilayered extensible Timoshenko microbeams", *J. Eng. Sci.*, **112**, 1-17. https://doi.org/10.1016/j.ijengsci.2016.09.007.

Farokhi, H. and Ghayesh, M.H. (2018), "Nonlinear mechanics of electrically actuated microplates", *J. Eng. Sci.*, **123**, 197-213. https://doi.org/10.1016/j.ijengsci.2017.08.017.

Farokhi, H. and Ghayesh, M.H. (2018), "Supercritical nonlinear parametric dynamics of Timoshenko microbeams", *Communication. Nonlinear. Sci. Numeric. Simul.*, **59**, 592-605. https://doi.org/10.1016/j.cnsns.2017.11.033.

Feli, S. and Jalilian, M.M. (2017), "Theoretical model of low-velocity impact on foam-core sandwich panels using finite difference method", *J. Sandwich Struct. Mater.,* **19**(3), 261-290. https://doi.org/10.1177/1099636216685316.

Gholami, R. and Ansari, R. (2018), "Nonlinear harmonically excited vibration of third-order shear deformable functionally graded graphene platelet-reinforced composite rectangular pates", *Eng. Struct.*, **156**, 197-209. https://doi.org/10.1016/j.engstruct.2017.11.019.

Ghayesh, M.H. (2018), "Functionally graded microbeams: Simultaneous presence of imperfection and viscoelasticity", *J. Mech. Sci*, **140**, 339-350. https://doi.org/10.1016/j.ijmecsci.2018.02.037.

Ghayesh, M.H., Farokhi, H. and Gholipour, A. (2017), "Vibration analysis of geometrically imperfect three-layered shear-deformable microbeams", *J. Mech. Sci.*, **122**, 370-383. https://doi.org/10.1016/j.ijmecsci.2017.01.001.

Ghayesh, M.H. (2018), "Nonlinear vibration analysis of axially functionally graded shear-deformable tapered beams", *Appl. Math. Model.*, **59**, 583-596. https://doi.org/10.1016/j.apm.2018.02.017.

Ghayesh, M.H. (2018), "Dynamics of functionally graded viscoelastic microbeams", *J. Eng. Sci.*, **124**, 115-131. https://doi.org/10.1016/j.ijengsci.2017.11.004.

Ghayesh, M.H. and Farokhi, H. (2015), "Chaotic motion of a parametrically excited microbeam", *J. Eng. Sci.*, **96**, 34-45. https://doi.org/10.1016/j.ijengsci.2015.07.004.

Ghayesh, M.H. and Farokhi, H., Alici, G. (2016), "Size-dependent performance of microgyroscopes", *J. Eng. Sci.*, **100**, 99-111. https://doi.org/10.1016/j.ijengsci.2015.11.003.

Ghayesh, M.H and Amabili, M., Farokhi, H. (2013), "Three-dimensional nonlinear size-dependent behaviour of Timoshenko microbeams", *J. Eng. Sci.*, **71**, 1-14. https://doi.org/10.1016/j.ijengsci.2013.04.003.

Ghayesh, M.H. and Farokhi, H. (2015), "Nonlinear dynamics of microplates", *J. Eng. Sci.*, **86**, 60-73. https://doi.org/10.1016/j.ijengsci.2014.10.004.

Ghayesh, M.H., Farokhi, H. and Amabili, M. (2013), "Nonlinear behaviour of electrically actuated MEMS resonators", *J. Eng. Sci.*, **71**, 137-155. https://doi.org/10.1016/j.ijengsci.2013.05.006.

Ghayesh, M.H., Amabili, M. and Farokhi, H. (2013), "Nonlinear forced vibrations of a microbeam based on the strain gradient elasticity theory", *J. Eng. Sci.*, **63**, 52-60. https://doi.org/10.1016/j.ijengsci.2012.12.001.

Ghayesh, M.H., Farokhi, H. and Gholipour, A. (2017), "Oscillations of functionally graded microbeams", *J. Eng. Sci.*, **110**, 35-53. https://doi.org/10.1016/j.ijengsci.2016.09.011.

Ghayesh, M.H., Farokhi, H., Gholipour, A. and Tavallaeinejad, M. (2018), "Nonlinear oscillations of functionally graded microplates", *J. Eng. Sci.*, **122**, 56-72. https://doi.org/10.1016/j.ijengsci.2017.03.014.

Gholipour, A., Farokhi, H. and Ghayesh, M.H. (2015), "In-plane and out-of-plane nonlinear size-dependent dynamics of microplates", *Nonlinear Dynam.*, **79**(3), 1771-1785. https://doi.org/10.1007/s11071-014-1773-7.

Ghayesh, M.H., Farokhi, H. and Amabili, M. (2013), "Nonlinear dynamics of a microscale beam based on the modified couple stress theory", *Compos. Part B*, **50**, 318-324.

https://doi.org/10.1016/j.compositesb.2013.02.021.

Ghayesh, M.H., Farokhi, H. and Amabili, M. (2014), “In-plane and out-of-plane motion characteristics of microbeams with modal interactions”, *Compos. Part B*, **60**, 423-439. https://doi.org/10.1016/j.compositesb.2013.12.074.

Heydari, M.M., Bidgoli, A.H., Golshani, H.R., Beygipoor, G. and Davoodi, A. (2015), “Nonlinear bending analysis of functionally graded CNT-reinforced composite Mindlin polymeric temperature-dependent plate resting on orthotropic elastomeric medium using GDQM”, *Nonlinear Dynam.*, **79**, 1425-1441. https://doi.org/10.1007/s11071-014-1751-0.

Kamil Żur, K. (2018), “Free vibration analysis of elastically supported functionally graded annular plates via quasi- Green’s function method”, *Compos. Part B*, **144**, 37-55. https://doi.org/10.1016/j.compositesb.2018.02.019.

Li, Q., Lu, V.P. and Kou, K.P. (2009), “Three-dimensional vibration analysis of functionally graded material sandwich plate”, *J. Sound Vib.*, **311,** 498-515. https://doi.org/10.1016/j.jsv.2007.09.018.

Mantari, J.L., Granados, E.V. and Guedes Soares, C. (2014), “Vibrational analysis of advanced composite plates resting on elastic foundation”, *Compos. Part B*, **66**, 407-419. https://doi.org/10.1016/j.compositesb.2014.05.026.

Mohammadzadeh, B. and Noh, H.C. (2014), “Use of buckling coefficient in predicting buckling load of plates with and without holes”, *J. Korean Soc. Adv. Compos. Struct.*, **5**(3), 1-7. http://dx.doi.org/10.11004/kosacs.2014.5.3.001.

Mohammadzadeh, B. and Noh, H.C. (2016), “Investigation into buckling coefficients of plates with holes considering variation of hole size and plate thickness”, *Mechanika,* **22**(3), 167-175. http://dx.doi.org/10.5755/j01.mech.22.3.12767.

Mohammadzadeh, B., Choi, E. and Kim, W.J. (2018), “Comprehensive investigation of buckling behavior of plates considering effects of holes”, *Struct. Eng. Mech.,* **68**(2)*,* 261-275. https://doi.org/10.12989/sem.2018.68.2.261.

Mohammadzadeh, B. (2016), “Investigation into dynamic responses of isotropic plates and sandwich plates subjected to blast loads”, Ph.D. Dissertation*,* Sejong University, Seoul, Korea.

Mohammadzadeh, B. and Noh, H.C. (2017), “Analytical method to investigate nonlinear dynamic responses of sandwich plates with FGM faces resting on elastic foundation considering blast loads”, *Compos. Struct.*, **174**, 142-157. https://doi.org/10.1016/j.compstruct.2017.03.087.

Mohammadzadeh, B. and Noh, H.C. (2015), “Numerical analysis of dynamic responses of the plate subjected to impulsive loads”, *J. Civil Environ. Struct. Construc. Arch. Eng.*, **9**(9), 1148-1151.

Mohammadzadeh, B., Bina, M. and Hasounizadeh, H. (2012), “Application and comparison of mathematical and physical models on inspecting slab of stilling basin floor under static and dynamic forces”, *Appl. Mech. Mater.*, **147**, 283-287. https://doi.org/10.4028/www.scientific.net/AMM.147.283.

Mohammadzadeh, B. and Noh, H.C. (2018), “An analytical and numerical investigations on the dynamic responses of steel plates considering the blast loads”, *J. Steel Struct.*, **19**, https://doi.org/10.1007/s13296-018-0150-7.

Mohammadzadeh, B. and Noh, H.C. (2014), “Investigation into central-difference and Newmark’s beta method in measuring dynamic responses”, *Adv. Mater. Res.*, **831**, 95-99.

Natarajan, S. and Manickam, G. (2012), “Bending and vibration of functionally graded material sandwich plates using an accurate theory”, *Finite Element Anal. Design*, **57**, 32-42. https://doi.org/10.1016/j.finel.2012.03.006.

Ninh, D.G. and Bich, D.H. (2016), “Nonlinear torsional bucklin and postbuckling of eccentrically stiffened ceramic functionally graded material metal layer cylindrical shell surrounded by elastic foundation subjected to thermo- mechanical load”, *J. Sandwich Struct. Mater.*, **18**(6), 712-738. https://doi.org/10.1177/1099636216644787.

Nguyen, T.N., Ngo, T.D. and Nguyen-Xuan, H. (2017), “A novel three-variable shear deformation plate formulation: theory and isogeometric implementation”, *Comput. Method Appl. Mech. Eng.,* **326**, 376-401. https://doi.org/10.1016/j.cma.2017.07.024.

Ngyuen, T.K., Ngyuen, V.H., Chau-Dinh, T., Vo, T.P. and Ngyuen-Xuan, H. (2016), “Static and vibration analysis of isotropic and functionally graded sandwich plates using an edge-based MITC3 finite elements”, *Compos. Part B,* **107**, 162-173. https://doi.org/10.1016/j.compositesb.2016.09.058.

Rajabi, M., Soltani, N. and Eshraghi, I. (2016), “Effects of temperature dependent material properties on mixed mode crack tip parameters of Functionally graded materials”, *Struct. Eng. Mech.*, **58**(2), 217-230. https://doi.org/10.12989/sem.2016.58.2.217.

Rajasekaran, S. (2013), “Free vibration of tapered arches made of axially Functionally graded materials”, *Struct. Eng. Mech.*, **45**(4), 569-594. https://doi.org/10.12989/sem.2013.45.4.569.

Ruocco, E., Zhang, H. and Wang, C.M. (2018), “Hencky bar-net model for buckling and vibration analysis of rectangular plates with non-uniform thickness”, *Eng. Struct.*, **168**, 653-668. https://doi.org/10.1016/j.engstruct.2018.04.080.

Shahrjerdi, A., Mustapha, F., Bayat, M., Sapuan, S.M., Zahari, R. and Shahzamaninan, M.M. (2011), “Natural frequency of F.G. rectangular plate by shear deformation theory”, *Mater. Sci. Eng.*, **17**, 166-175.

Shariyat, M., Khalili, S.M.R. and Rajabi, I. (2015), “A global-local theory with stress recovery and a new post-processing technique for stress analysis of asymmetric orthotropic sandwich plates with single/dual cores”, *Comput. Method Appl. Mech. Eng.*, **286,** 192-215. https://doi.org/10.1016/j.cma.2014.12.015.

Soni, S., Jain, N.K. and Joshi, P.V. (2017), “Analytical modeling for nonlinear vibration analysis of partially cracked thin magneto-electro-elastic plate coupled with fluid”, *Nonlinear Dynam.*, **90**, 137-170. https://doi.org/10.1007/s11071-017-3652-5.

Trinh, L.C., Vo, T.P., Thai, H.T., Nguyen, T.K. and Keerthan, P. (2018), “State-space Levy solution for size-dependent static, free vibration and buckling behaviours of functionally graded sandwich plates”, *Compos. Part B*, **149**, 144-164. https://doi.org/10.1016/j.compositesb.2018.05.017.

Vafakhah, Z. and Navayi Neya, B. (2019), “An exact three-dimensional solution for bending of thick rectangular FGM plate”, *Compos. Part B*, **156**, 72-87. https://doi.org/10.1016/j.compositesb.2018.08.036.

Wang, Z.X. and Shen, H.S. (2011), “Nonlinear analysis of sandwich plates with FGM face sheets resting on elastic foundation”, *Compos. Struct.*, **93,** 2521-2532. https://doi.org/10.1016/j.compstruct.2011.04.014.

Wang, Y.Q. and Zu, J.W. (2017), “Nonlinear dynamic thermoelastic response of rectangular FGM plates with longitudinal velocity”, *Compos. Part B,* **117**, 74-88. https://doi.org/10.1016/j.compositesb.2017.02.037.

Wang, Y.Q. and Zu, J.W. (2017), “Nonlinear steady-state responses of longitudinally traveling functionally graded material plates in contact with liquid”, *Compos. Struct.*, **164**, 130-144. https://doi.org/10.1016/j.compstruct.2016.12.053.

Wang, Y.Q., Ye, C. and Zu, J.W. (2018), “Identifying the temperature effect on the vibrations of functionally graded cylindrical shells with porosities”, *Appl. Math. Mech.*, **39**(11), 1587-1604. https://doi.org/10.1007/s10483-018-2388-6.

Wang, Y.Q. and Zu, J.W. (2017), “Vibration behaviors of functionally graded rectangular plates with porosities and moving in thermal environment”, *Aerosp. Sci. Technol.,* **69**, 550-562. https://doi.org/10.1016/j.ast.2017.07.023.

Wang, Y.Q. (2018), “Electro-mechanical vibration analysis of

functionally graded piezoelectric porous plates in the translation state", *Acta Astronautica*, **143**, 263-271. https://doi.org/10.1016/j.actaastro.2017.12.004.
Wang, Y.Q., Huang, X.B. and Li, J. (2016), "Hydroelastic dynamic analysis of axially moving plates in continuous hot-dip galvanizing process", *J. Mech. Sci.*, **110**, 201-216. https://doi.org/10.1016/j.ijmecsci.2016.03.010.
Wang, Y.Q., Li, H.H., Zhang, Y.F. and Zu, J.W. (2018), "A nonlinear surface-stress-dependent model for vibration analysis of cylindrical nanoscale shells conveying fluid", *Appl. Math. Model.*, **64**, 55-70. https://doi.org/10.1016/j.apm.2018.07.016.
Wang, Y.Q., Wan, Y.H. and Zu, J. (2019), "Nonlinear dynamic characteristics of functionally graded sandwich thin nanoshells conveying fluid incorporating surface stress influence", *Thin Wall Struct.*, **135**, 537-547. https://doi.org/10.1016/j.tws.2018.11.023.
Wang, Y.Q. and Yang, Z. (2017), "Nonlinear vibrations of moving functionally graded plates containing porosities and contacting with liquid: internal resonance", *Nonlinear Dynam.*, **90**, 1461-1480. https://doi.org/10.1007/s11071-017-3739-z.
Wang, Y.Q. and Zu, J.W. (2017), "Analytical analysis for vibration of longitudinally moving plate submerged in infinite liquid domain", *Appl. Math. Mech.*, **38**, 625-646. https://doi.org/10.1007/s10483-017-2192-9.
Wang, Y.Q., Ye, C. and Zu, J. (2019), "Nonlinear vibration of metal foam cylindrical shells reinforced with graphene platelets", *Aerosp. Sci. Technol.*, **85**, 359-370. https://doi.org/10.1016/j.ast.2018.12.022.
Wang, Y.Q. and Zu, J.W. (2018), "Nonlinear Dynamics of a Translational FGM Plate with Strong Mode Interaction", *J. Struct. Stability Dynam.*, **18**, 1850031. https://doi.org/10.1142/S0219455418500311.
Wang, Y.Q., Liang, L. and Guo, X.H. (2013), "Internal resonance of axially moving laminated circular cylindrical shells", *J. Sound Vib.*, **332**, 6434-6450. https://doi.org/10.1016/j.jsv.2013.07.007.
Wang, Y.Q. (2014), "Nonlinear vibration of a rotating laminated composite circular cylindrical shell: traveling wave vibration", *Nonlinear Dynam.*, **77**, 1693-1707. https://doi.org/10.1007/s11071-014-1410-5.
Wang, Y.Q. and Zu, J.W. (2017), "Instability of Viscoelastic Plates with Longitudinally Variable Speed and Immersed in Ideal Liquid", *J. Appl. Mech.*, **9**(1), 1750005. https://doi.org/10.1142/S1758825117500053.
Yang, C., Chen, J. and Zhao, S. (2013), "The interlaminar stress of laminated composite under uniform axial deformation", *Modeling Numeric. Simul. Mater. Sci.*, **3**, 49-60. http://dx.doi.org/10.4236/mnsms.2013.32007.
Zamani Nejad, M., Hadi, A. and Farajpour, A. (2017), "Consistent couple-stress theory for free vibration analysis of Euler-Bernoulli nano-beams made of arbitrary bi-directional Functionally graded materials", *Struct. Eng. Mech.*, **63**(2), 161-169. https://doi.org/10.12989/sem.2017.63.2.161.
Zhou, K., Huang, X., Tian, J. and Hua, H. (2018) "Vibration and flutter analysis of supersonic porous functionally graded material plates with temperature gradient and resting on elastic foundation", *Compos. Struct.*, **204**, 63-79. https://doi.org/10.1016/j.compstruct.2018.07.057.

CC

Nomenclature

t	time
$\omega_{\kappa\lambda}$	Natural frequency
$[K]$	stiffness matrix
[M]	mass matrix
$[\chi]$	coefficient matrix
M	mass
E	modulus of elasticity
ν	Poisson's ratio
ρ	material density
G	shear modulus of elasticity
κ	curvature
I_{ji}	mass moment of inertias
q_x	distributed load along x-direction
q_y	distributed load along y-direction
q_b	distributed forces at bottom layer
q_t	distributed forces at top layer
N_m	membrane force
M_b	bending moment
P	higher order bending moment
Q	shear force
R	higher order shear moment
$\bar{N}^T$	thermal force
$\bar{M}^T$	thermal moment
$\bar{P}^T$	thermal higher order moment
Ω_0	plate area
σ	stress
σ^T	thermal stress
ε	strain
γ	shear strain
a	length of plate (long side)
c	width of plate (short side)
h	thickness of plate
h_f	thickness of face sheet
h_{frc}	thickness of core
t_i	layer height through the plate thickness
P_F	effective material properties
P_c	temperature-dependent properties of ceramic
P_m	temperature-dependent properties of metal
V_c	volume fraction of ceramic
V_m	volume fraction of metal
Z	depth through the plate thickness
A_M	cross-sectional area of matrix
A_r	cross-sectional area of reinforcement
A_c	cross-sectional area of composite
N	volume fraction index
α	thermal expansion coefficient
$\bar{Q}_{ij}$	constitutive stiffness matrix element
U	displacement in x-direction
V	displacement in y-direction
W	displacement in z-direction
Ψ_x	rotation in y-direction
Ψ_y	rotation in x-direction
$\dot{U}$	time-derivative of U
$\dot{V}$	time-derivative of V
$\dot{W}$	time-derivative of W
$\dot{\Psi}_x$	time-derivative of Ψ_x

$\dot{\Psi}_y$	time-derivative of Ψ_y
$\ddot{U}$	second time-derivative of U
$\ddot{V}$	second time-derivative of V
$\ddot{W}$	second time-derivative of W
$\ddot{\Psi}_x$	second time-derivative of Ψ_x
$\ddot{\Psi}_y$	second time-derivative of Ψ_y
K_1	Winkler foundation stiffness
K_2	shear layer stiffness
ρ_0	$1\ {kg}/{m^3}$
E_0	1 GPa
U_{se}	strain energy
V_{ew}	external work
K_e	kinetic energy

Appendix A: Coefficients for equations of Frequency

For simplicity and neat appearance, $\omega_{\kappa\lambda}$ is replaced by ω.

$c_1 = \sum_{i=1}^{\aleph}\Big[(\bar{Q}_{16})_i\frac{4\pi^2h_i}{ac}\cos\frac{2\pi x}{a}\sin\frac{2\pi y}{c} -$
$(\bar{Q}_{11})_i\frac{4\pi^2h_i}{a^2}\sin\frac{2\pi x}{a}\left(1-\cos\frac{2\pi y}{c}\right) +$
$(\bar{Q}_{66})_i\frac{4\pi^2h_i}{c^2}\sin\frac{2\pi x}{a}\cos\frac{2\pi y}{c} +$
$(\bar{Q}_{16})_i\frac{4\pi^2h_i}{ac}\cos\frac{2\pi x}{a}\sin\frac{2\pi y}{c}\Big]e^{-i\omega t}$

$c_2 = \sum_{i=1}^{\aleph}\Big[(\bar{Q}_{12})_i\frac{4\pi^2h_i}{ac}\sin\frac{2\pi x}{a}\cos\frac{2\pi y}{c} - (\bar{Q}_{26})_i\frac{4\pi^2h_i}{c^2}\Big(1-$
$\cos\frac{2\pi x}{a}\Big)\sin\frac{2\pi y}{c} + (\bar{Q}_{66})_i\frac{4\pi^2h_i}{ac}\sin\frac{2\pi x}{a}\cos\frac{2\pi y}{c} +$
$(\bar{Q}_{16})_i\frac{4\pi^2h_i}{a^2}\cos\frac{2\pi x}{a}\sin\frac{2\pi y}{c}\Big]e^{-i\omega t}$

$c_3 = \sum_{i=1}^{\aleph}\Big[(\bar{Q}_{16})_i\frac{8\pi^3h_i^2}{3a^2c}\cos\frac{2\pi x}{a}\sin\frac{2\pi y}{c} + (\bar{Q}_{26})_i\frac{8\pi^3h_i^2}{3c^3}\Big(1-$
$\cos\frac{2\pi x}{a}\Big)\sin\frac{2\pi y}{c} - (\bar{Q}_{66}+\bar{Q}_{12})_i\frac{8\pi^3h_i^2}{3ac^2}\sin\frac{2\pi x}{a}\cos\frac{2\pi y}{c} -$
$(\bar{Q}_{11})_i\frac{8\pi^3h_i^2}{3a^3}\sin\frac{2\pi x}{a}\left(1-\cos\frac{2\pi y}{c}\right) -$
$(\bar{Q}_{16})_i\frac{16\pi^3h_i^2}{3ac^2}\cos\frac{2\pi x}{a}\sin\frac{2\pi y}{c}\Big]e^{-i\omega t}$

$$c_4 = \sum_{i=1}^{\aleph}\Bigg[(\bar{Q}_{16})_i\frac{8\pi^3h_i}{ca^2}\sin^2\frac{2\pi x}{a}\left(1-\cos\frac{2\pi y}{c}\right)\sin\frac{2\pi y}{c}$$
$$+ (\bar{Q}_{26})_i\frac{8\pi^3h_i}{c^3}\left(1-\cos\frac{2\pi x}{a}\right)^2\cos\frac{2\pi y}{c}\sin\frac{2\pi y}{c}$$
$$+ (\bar{Q}_{66})_i\frac{8\pi^3h_i}{ac^2}\sin\frac{2\pi x}{a}\left(1-\cos\frac{2\pi x}{a}\right)\Big(1$$
$$-\cos\frac{2\pi y}{c}\Big)\cos\frac{2\pi y}{c}$$
$$+ (\bar{Q}_{11})_i\frac{8\pi^3h_i}{a^3}\cos\frac{2\pi x}{a}\sin\frac{2\pi x}{a}\left(1-\cos\frac{2\pi y}{c}\right)^2$$
$$+ (\bar{Q}_{12})_i\frac{8\pi^3h_i}{ac^2}\sin^2\frac{2\pi y}{c}\sin\frac{2\pi x}{a}\left(1-\cos\frac{2\pi x}{a}\right)$$
$$- (\bar{Q}_{16})_i\frac{8\pi^3h_i}{a^2c}\cos\frac{2\pi x}{a}\left(1-\cos\frac{2\pi x}{a}\right)\Big(1$$
$$-\cos\frac{2\pi y}{c}\Big)\sin\frac{2\pi y}{c}\Bigg]e^{-2i\omega t}$$

$c_5 = \sum_{i=1}^{\aleph}\Big[(\bar{Q}_{16})_i\frac{4\pi^2h_i^2}{3ac}\cos\frac{2\pi x}{a}\sin\frac{2\pi y}{c} +$
$(\bar{Q}_{66})_i\frac{2\pi^2h_i^2}{3c^2}\sin\frac{2\pi x}{a}\cos\frac{2\pi y}{c} - (\bar{Q}_{11})_i\frac{2\pi^2h_i^2}{3a^2}\sin\frac{2\pi x}{a}\Big(1-$
$\cos\frac{2\pi y}{c}\Big)\Big]e^{-i\omega t}$

$c_6 = \sum_{i=1}^{\aleph}\Big[(\bar{Q}_{26})_i\frac{2\pi^2h_i^2}{3c^2}\left(1-\cos\frac{2\pi x}{a}\right)\cos\frac{2\pi y}{c} + (\bar{Q}_{66}+$
$\bar{Q}_{12})_i\frac{2\pi^2h_i^2}{3ac}\sin\frac{2\pi x}{a}\cos\frac{2\pi y}{c} +$
$(\bar{Q}_{16})_i\frac{2\pi^2h_i^2}{3a^2}\cos\frac{2\pi x}{a}\sin\frac{2\pi y}{c}\Big]e^{-i\omega t}$

$c_7 = \sum_{i=1}^{\aleph}\Big[I_{0i}\sin\frac{2\pi x}{a}\left(1-\cos\frac{2\pi y}{c}\right)\Big]\omega^2e^{-i\omega t}$

$c_8 = \sum_{i=1}^{\aleph}\Big[\left(I_{1i}-\frac{4}{3h^2}I_{3i}\right)\sin\frac{2\pi x}{a}\left(1-\cos\frac{2\pi y}{c}\right)\Big]\omega^2e^{-i\omega t}$

$c_9 = \sum_{i=1}^{\aleph}\Big[\frac{8\pi}{3ah_i^2}I_{3i}\sin\frac{2\pi x}{a}\left(1-\cos\frac{2\pi y}{c}\right)\Big]\omega^2e^{-i\omega t}$

$c_{10} = \sum_{i=1}^{\aleph}(\bar{Q}_{11}\alpha_{11}+\bar{Q}_{12}\alpha_{22})_ih_i$

$c_{11} = \sum_{i=1}^{\aleph}(\bar{Q}_{16}\alpha_{11}+\bar{Q}_{26}\alpha_{22})_ih_i$

$d_1 = \sum_{i=1}^{\aleph}\Big[(\bar{Q}_{12})_i\frac{4\pi^2h_i}{ac}\cos\frac{2\pi x}{a}\sin\frac{2\pi y}{c} -$
$(\bar{Q}_{16})_i\frac{4\pi^2h_i}{a^2}\sin\frac{2\pi x}{a}\left(1-\cos\frac{2\pi y}{c}\right) +$
$(\bar{Q}_{26})_i\frac{4\pi^2h_i}{c^2}\sin\frac{2\pi x}{a}\cos\frac{2\pi y}{c} +$
$(\bar{Q}_{66})_i\frac{4\pi^2h_i}{ac}\cos\frac{2\pi x}{a}\sin\frac{2\pi y}{c}\Big]e^{-i\omega t}$

$d_2 = \sum_{i=1}^{\aleph}\Big[(\bar{Q}_{26})_i\frac{4\pi^2h_i}{ac}\sin\frac{2\pi x}{a}\cos\frac{2\pi y}{c} - (\bar{Q}_{22})_i\frac{4\pi^2h_i}{c^2}\Big(1-$
$\cos\frac{2\pi x}{a}\Big)\sin\frac{2\pi y}{c} + (\bar{Q}_{26})_i\frac{4\pi^2h_i}{ac}\sin\frac{2\pi x}{a}\cos\frac{2\pi y}{c} +$
$(\bar{Q}_{66})_i\frac{4\pi^2h_i}{a^2}\cos\frac{2\pi x}{a}\sin\frac{2\pi y}{c}\Big]e^{-i\omega t}$

$d_3 = \sum_{i=1}^{\aleph}\Big[(\bar{Q}_{12})_i\frac{8\pi^3h_i^2}{3a^2c}\cos\frac{2\pi x}{a}\sin\frac{2\pi y}{c} + (\bar{Q}_{22})_i\frac{8\pi^3h_i^2}{3c^3}\Big(1-$
$\cos\frac{2\pi x}{a}\Big)\sin\frac{2\pi y}{c} - (\bar{Q}_{26})_i\frac{16\pi^3h_i^2}{3ac^2}\sin\frac{2\pi x}{a}\cos\frac{2\pi y}{c} -$
$(\bar{Q}_{16})_i\frac{8\pi^3h_i^2}{3a^3}\sin\frac{2\pi x}{a}\left(1-\cos\frac{2\pi y}{c}\right) -$
$(\bar{Q}_{66})_i\frac{16\pi^3h_i^2}{3ac^2}\cos\frac{2\pi x}{a}\sin\frac{2\pi y}{c}\Big]e^{-i\omega t}$

$d_4 = \sum_{i=1}^{\aleph}\Big[(\bar{Q}_{12})_i\frac{8\pi^3h_i}{ca^2}\sin^2\frac{2\pi x}{a}\left(1-\cos\frac{2\pi y}{c}\right)\sin\frac{2\pi y}{c} +$
$(\bar{Q}_{22})_i\frac{8\pi^3h_i}{c^3}\left(1-\cos\frac{2\pi x}{a}\right)^2\cos\frac{2\pi y}{c}\sin\frac{2\pi y}{c} +$
$(\bar{Q}_{26})_i\frac{8\pi^3h_i}{ac^2}\sin\frac{2\pi x}{a}\left(1-\cos\frac{2\pi x}{a}\right)\left(1-\cos\frac{2\pi y}{c}\right)\cos\frac{2\pi y}{c} +$
$(\bar{Q}_{16})_i\frac{8\pi^3h_i}{a^3}\cos\frac{2\pi x}{a}\sin\frac{2\pi x}{a}\left(1-\cos\frac{2\pi y}{c}\right)^2 +$
$(\bar{Q}_{26})_i\frac{8\pi^3h_i}{ac^2}\sin^2\frac{2\pi y}{c}\sin\frac{2\pi x}{a}\left(1-\cos\frac{2\pi x}{a}\right) -$
$(\bar{Q}_{66})_i\frac{8\pi^3h_i}{a^2c}\cos\frac{2\pi x}{a}\left(1-\cos\frac{2\pi x}{a}\right)\Big(1-$
$\cos\frac{2\pi y}{c}\Big)\sin\frac{2\pi y}{c}\Big]e^{-2i\omega t}$

$d_5 = \sum_{i=1}^{\aleph}\Big[(\bar{Q}_{12})_i\frac{2\pi^2h_i^2}{3ac}\cos\frac{2\pi x}{a}\sin\frac{2\pi y}{c} +$
$(\bar{Q}_{26})_i\frac{2\pi^2h_i^2}{3c^2}\sin\frac{2\pi x}{a}\cos\frac{2\pi y}{c} - (\bar{Q}_{16})_i\frac{2\pi^2h_i^2}{3a^2}\sin\frac{2\pi x}{a}\Big(1-$
$\cos\frac{2\pi y}{c}\Big) - (\bar{Q}_{66})_i\frac{4\pi^2h_i^2}{3ac}\cos\frac{2\pi x}{a}\sin\frac{2\pi y}{c}\Big]e^{-i\omega t}$

$d_6 = \sum_{i=1}^{\aleph}\Big[(\bar{Q}_{22})_i \frac{2\pi^2 h_i^2}{3c^2}\left(1 - cos\frac{2\pi x}{a}\right) cos\frac{2\pi y}{c} + (\bar{Q}_{26})_i \frac{4\pi^2 h_i^2}{3ac} sin\frac{2\pi x}{a} cos\frac{2\pi y}{c} + (\bar{Q}_{66})_i \frac{2\pi^2 h_i^2}{3a^2} cos\frac{2\pi x}{a} sin\frac{2\pi y}{c}\Big] e^{-i\omega t}$

$d_7 = \sum_{i=1}^{\aleph}\left[I_{0i}\left(1 - cos\frac{2\pi x}{a}\right) sin\frac{2\pi y}{c}\right] \omega^2 e^{-i\omega t}$

$d_8 = \sum_{i=1}^{\aleph}\left[\left(I_{1i} - \frac{4}{3h^2} I_{3i}\right)\left(1 - cos\frac{2\pi x}{a}\right) sin\frac{2\pi y}{c}\right] \omega^2 e^{-i\omega t}$

$d_9 = \sum_{i=1}^{\aleph}\left[\frac{8\pi}{3bh_i^2} I_{3i}\left(1 - cos\frac{2\pi x}{a}\right) sin\frac{2\pi y}{c}\right] \omega^2 e^{-i\omega t}$

$d_{10} = \sum_{i=1}^{\aleph}(\bar{Q}_{12}\alpha_{11} + \bar{Q}_{22}\alpha_{22})_i h_i$

$d_{11} = \sum_{i=1}^{\aleph}(\bar{Q}_{16}\alpha_{11} + \bar{Q}_{26}\alpha_{22})_i h_i$

$e_1 = \sum_{i=1}^{\aleph}\Big[(Q_{11})_i \frac{4\pi^3 h_i}{3a^3}(2h_i - 3) sin^2\frac{2\pi x}{a}\left(1 - cos\frac{2\pi y}{c}\right)^2 + (Q_{16})_i \frac{4\pi^3 h_i}{3a^2 c}(3 - 2h_i) sin\frac{2\pi x}{a}\left(5cos\frac{2\pi x}{a} - 2\right) sin\frac{2\pi y}{c}\left(1 - cos\frac{2\pi y}{c}\right) + \left(Q_{66} + \frac{1}{2}Q_{12}\right)_i \frac{8\pi^3 h_i}{3ac^2}(3 - 2h_i) cos\frac{2\pi x}{a}\left(1 - cos\frac{2\pi x}{a}\right) sin^2\frac{2\pi y}{c} + (Q_{26})_i \frac{4\pi^3 h_i}{3c^3}(3 - 2h_i) sin\frac{2\pi x}{a}\left(1 - cos\frac{2\pi x}{a}\right) sin\frac{2\pi y}{c} cos\frac{2\pi y}{c} + (Q_{66})_i \frac{8\pi^3 h_i}{3ac^2}(3 - 2h_i) sin^2\frac{2\pi x}{a} cos\frac{2\pi y}{c}\left(1 - cos\frac{2\pi y}{c}\right)\Big] e^{-2i\omega t}$

$e_2 = \sum_{i=1}^{\aleph}\Big[\left(Q_{66} + \frac{1}{2}Q_{12}\right)_i \frac{8\pi^3 h_i}{3a^2 c}(3 - 2h_i) sin^2\frac{2\pi x}{a} cos\frac{2\pi y}{c}\left(1 - cos\frac{2\pi y}{c}\right) + (Q_{16})_i \frac{4\pi^3 h_i}{3a^3}(3 - 2h_i) sin\frac{2\pi x}{a} cos\frac{2\pi x}{a} sin\frac{2\pi y}{c}\left(1 - cos\frac{2\pi y}{c}\right) + (Q_{26})_i \frac{4\pi^3 h_i}{3ac^2}(3 - 2h_i) sin\frac{2\pi x}{a}\left(1 - cos\frac{2\pi x}{a}\right) sin\frac{2\pi y}{c}\left(5cos\frac{2\pi y}{c} - 2\right) + (Q_{66})_i \frac{8\pi^3 h_i}{3a^2 c}(3 - 2h_i) cos\frac{2\pi x}{a}\left(1 - cos\frac{2\pi x}{a}\right) sin^2\frac{2\pi y}{c} + (Q_{22})_i \frac{4\pi^3 h_i}{3c^3}(3 - 2h_i) sin\frac{2\pi x}{a}\left(1 - cos\frac{2\pi x}{a}\right) sin\frac{2\pi y}{c}\left(1 - cos\frac{2\pi y}{c}\right)\Big] e^{-2i\omega t}$

$e_3 = \sum_{i=1}^{\aleph}\Big[(Q_{11})_i \frac{\pi^3 h_i^2}{315a^3}(32h_i - 210) sin^2\frac{2\pi x}{a}\left(1 - cos\frac{2\pi y}{c}\right)^2 + (Q_{16})_i \frac{3\pi^3 h_i^2}{315a^2 c}(210 - 32h_i) sin\frac{2\pi x}{a} cos\frac{2\pi x}{a} sin\frac{2\pi y}{c}\left(1 - cos\frac{2\pi y}{c}\right) + (Q_{12} + 2Q_{66})_i \frac{\pi^3 h^2}{315ac^2}(210 - 32h_i) cos\frac{2\pi x}{a}\left(1 - cos\frac{2\pi x}{a}\right) sin^2\frac{2\pi y}{c} + (Q_{26})_i \frac{\pi^3 h^2}{315c^3}(210 - 32h_i) sin\frac{2\pi x}{a}\left(1 - cos\frac{2\pi x}{a}\right) sin\frac{2\pi y}{c} cos\frac{2\pi y}{c} + (Q_{66})_i \frac{2\pi^3 h_i^2}{3ac^2}(210 - 32h_i) sin^2\frac{2\pi x}{a} cos\frac{2\pi y}{c}\left(1 - cos\frac{2\pi y}{c}\right) + (Q_{16})_i \frac{2\pi^3 h^2}{315a^2 c}(210 - 32h_i) sin\frac{2\pi x}{a}\left(1 - cos\frac{2\pi x}{a}\right) sin\frac{2\pi y}{c}\left(1 - cos\frac{2\pi y}{c}\right)\Big] e^{-2i\omega t}$

$e_4 = \sum_{i=1}^{\aleph}\Big[(Q_{12} + 2Q_{66})_i \frac{\pi^3 h_i^2}{315a^2 c}(210 - 32h_i) sin^2\frac{2\pi x}{a} cos\frac{2\pi y}{c}\left(1 - cos\frac{2\pi y}{c}\right) + (Q_{16})_i \frac{\pi^3 h_i^2}{315a^3}(210 - 32h_i) sin\frac{2\pi x}{a} cos\frac{2\pi x}{a} sin\frac{2\pi y}{c}\left(1 - cos\frac{2\pi y}{c}\right) + (Q_{26})_i \frac{3\pi^3 h_i^2}{315ac^2}(210 - 32h_i) sin\frac{2\pi x}{a}\left(1 - cos\frac{2\pi x}{a}\right) sin\frac{2\pi y}{c} cos\frac{2\pi y}{c} + (Q_{66})_i \frac{2\pi^3 h_i^2}{315a^2 c}(210 - 32h_i) cos\frac{2\pi x}{a}\left(1 - cos\frac{2\pi x}{a}\right) sin^2\frac{2\pi y}{c} + (Q_{22})_i \frac{\pi^3 h_i^2}{315c^3}(210 - 32h_i)\left(1 - cos\frac{2\pi x}{a}\right)^2 sin\frac{2\pi y}{c} cos\frac{2\pi y}{c} + (Q_{26})_i \frac{2\pi^3 h_i^2}{315ac^2}(210 - 32h_i) sin\frac{2\pi x}{a}\left(1 - cos\frac{2\pi x}{a}\right) cos\frac{2\pi y}{c}\left(1 - cos\frac{2\pi y}{c}\right)\Big] e^{-2i\omega t}$

$e_5 = \sum_{i=1}^{\aleph}\Big[(2Q_{45})_i \frac{92\pi^2 h_i}{15ac} sin\frac{2\pi x}{a} sin\frac{2\pi y}{c} - (Q_{55})_i \frac{92\pi^2 h_i}{15a^2} cos\frac{2\pi x}{a}\left(1 - cos\frac{2\pi y}{c}\right) + (Q_{44})_i \frac{92\pi^2 h_i}{15c^2}\left(1 - cos\frac{2\pi x}{a}\right) cos\frac{2\pi y}{c}\Big] e^{-i\omega t}$

$e_6 = \sum_{i=1}^{\aleph}\Big[(Q_{11})_i \frac{8\pi^4 h_i^2}{63a^4}(32h_i - 21) sin^2\frac{2\pi x}{a}\left(1 - cos\frac{2\pi y}{c}\right)^2 + (Q_{12})_i \frac{8\pi^4 h_i^2}{63a^2 c^2}(32h_i - 21) sin^2\frac{2\pi x}{a} cos\frac{2\pi y}{c}\left(1 - cos\frac{2\pi y}{c}\right) + (Q_{16})_i \frac{16\pi^4 h_i^2}{63a^3 c}(32h_i - 21) sin\frac{2\pi x}{a}\left(1 - cos\frac{2\pi x}{a}\right) sin\frac{2\pi y}{c}\left(1 - cos\frac{2\pi y}{c}\right) + (Q_{66})_i \frac{32\pi^4 h_i^2}{63a^2 c^2}(32h_i - 1) cos\frac{2\pi x}{a}\left(1 - cos\frac{2\pi x}{a}\right) sin^2\frac{2\pi y}{c} + (Q_{22})_i \frac{8\pi^4 h_i^2}{63c^2}(21 - 32h_i)\left(1 - cos\frac{2\pi x}{a}\right)^2 sin^2\frac{2\pi y}{c} + (Q_{66})_i \frac{16\pi^4 h_i^2}{63a^2 c^2}(64h_i - 1) sin^2\frac{2\pi x}{a} cos\frac{2\pi y}{c}\left(1 - cos\frac{2\pi y}{c}\right) + (Q_{12})_i \frac{8\pi^4 h_i^2}{63a^2 c^2}(21 - 32h_i) cos\frac{2\pi x}{a}\left(1 - cos\frac{2\pi x}{a}\right) sin^2\frac{2\pi y}{c} + (Q_{26})_i \frac{16\pi^4 h_i^2}{3ac^3}(21 - 32h_i) sin\frac{2\pi x}{a}\left(1 - cos\frac{2\pi x}{a}\right) sin\frac{2\pi y}{c}\left(1 - cos\frac{2\pi y}{c}\right) + (Q_{26})_i \frac{8\pi^4 h_i^2}{3ac^3}(64h_i - 3) sin\frac{2\pi x}{a}\left(1 - cos\frac{2\pi x}{a}\right) sin\frac{2\pi y}{c} cos\frac{2\pi y}{c}\Big] e^{-2i\omega t}$

$e_7 = \sum_{i=1}^{\aleph}\Big[(Q_{11})_i \frac{8\pi^4 h_i}{3a^4}(3 - 2h_i) sin^2\frac{2\pi x}{a} cos\frac{2\pi x}{a}\left(1 - cos\frac{2\pi y}{c}\right)^3 + (2Q_{12})_i \frac{8\pi^4 h_i}{3a^2 c^2}(3 - 2h_i) sin^2\frac{2\pi x}{a} sin^2\frac{2\pi y}{c}\left(1 -\right.$

$cos\frac{2\pi x}{a}\Big)\Big(1-cos\frac{2\pi y}{c}\Big)+(Q_{16})_i\frac{16\pi^4 h_i}{3ac^3}(3-2h_i)sin\frac{2\pi x}{a}cos\frac{2\pi x}{a}\Big(1-cos\frac{2\pi x}{a}\Big)\Big(1-cos\frac{2\pi y}{c}\Big)^2 sin\frac{2\pi y}{c}+(Q_{26})_i\frac{16\pi^4 h_i}{3ac^3}(3-2h_i)sin\frac{2\pi x}{a}\Big(1-cos\frac{2\pi x}{a}\Big)^2 sin^3\frac{2\pi y}{c}+(Q_{66})_i\frac{16\pi^4 h_i}{3a^2c^2}(3-2h_i)cos\frac{2\pi x}{a}\Big(1-cos\frac{2\pi x}{a}\Big)^2 sin^2\frac{2\pi y}{c}\Big(1-cos\frac{2\pi y}{c}\Big)+(Q_{22})_i\frac{8\pi^4 h_i}{3c^4}(3-2h_i)\Big(1-cos\frac{2\pi x}{a}\Big)^3 sin^2\frac{2\pi y}{c}cos\frac{2\pi y}{c}+(Q_{26})_i\frac{8\pi^4 h_i}{3ac^3}(3-2h_i)sin\frac{2\pi x}{a}\Big(1-cos\frac{2\pi x}{a}\Big)^2 sin\frac{2\pi y}{c}cos\frac{2\pi y}{c}\Big(1-cos\frac{2\pi y}{c}\Big)+(Q_{16})_i\frac{16\pi^4 h_i}{3a^3c}(3-2h_i)sin^3\frac{2\pi x}{a}sin\frac{2\pi y}{c}\Big(1-cos\frac{2\pi y}{c}\Big)^2+(Q_{26})_i\frac{16\pi^4 h_i}{3ac^3}(3-2h_i)sin\frac{2\pi x}{a}\Big(1-cos\frac{2\pi x}{a}\Big)^2 sin\frac{2\pi y}{c}cos\frac{2\pi y}{c}\Big(1-cos\frac{2\pi y}{c}\Big)+(Q_{66})_i\frac{16\pi^4 h_i}{3a^2c^2}(3-2h_i)sin^2\frac{2\pi x}{a}\Big(1-cos\frac{2\pi x}{a}\Big)cos\frac{2\pi y}{c}\Big(1-cos\frac{2\pi y}{c}\Big)^2\Big]e^{-3i\omega t}$

$e_8=\sum_{i=1}^{\aleph}\Big[(Q_{55})_i\frac{46\pi h_i}{15a}cos\frac{2\pi x}{a}\Big(1-cos\frac{2\pi y}{c}\Big)+(Q_{45})_i\frac{46\pi h_i}{15b}sin\frac{2\pi x}{a}sin\frac{2\pi y}{c}\Big]e^{-i\omega t}$

$e_9=\sum_{i=1}^{\aleph}\Big[(Q_{44})_i\frac{46\pi h_i}{15c}\Big(1-cos\frac{2\pi x}{a}\Big)cos\frac{2\pi y}{c}+(Q_{45})_i\frac{46\pi h_i}{15a}sin\frac{2\pi x}{a}sin\frac{2\pi y}{c}\Big]e^{-i\omega t}$

$e_{10}=\sum_{i=1}^{\aleph}\Big[I_{0i}\Big(1-cos\frac{2\pi x}{a}\Big)\Big(1-cos\frac{2\pi y}{c}\Big)-\frac{32\pi I_{6i}}{9h_i^4}\Big(\frac{1}{a}sin\frac{2\pi x}{a}\Big(1-cos\frac{2\pi y}{c}\Big)+\frac{1}{b}\Big(1-cos\frac{2\pi x}{a}\Big)sin\frac{2\pi y}{c}\Big)\Big]\omega^2 e^{-i\omega t}$

$e_{11}=\sum_{i=1}^{\aleph}\Big[I_{3i}\frac{8\pi}{3ah_i^2}cos\frac{2\pi x}{a}\Big(1-cos\frac{2\pi y}{c}\Big)\Big]\omega^2 e^{-i\omega t}$

$e_{12}=\sum_{i=1}^{\aleph}\Big[I_{3i}\frac{8\pi}{3bh_i^2}\Big(1-cos\frac{2\pi x}{a}\Big)cos\frac{2\pi y}{c}\Big]\omega^2 e^{-i\omega t}$

$e_{13}=\sum_{i=1}^{\aleph}\Big[\Big(\frac{8\pi I_{4i}}{3ah_i^2}+\frac{32\pi I_{6i}}{9ah_i^2}\Big)cos\frac{2\pi x}{a}\Big(1-cos\frac{2\pi y}{c}\Big)\Big]\omega^2 e^{-i\omega t}$

$e_{14}=\sum_{i=1}^{\aleph}\Big[\Big(\frac{8\pi I_{4i}}{3ah_i^2}+\frac{32\pi I_{6i}}{9ah_i^2}\Big)\Big(1-cos\frac{2\pi x}{a}\Big)cos\frac{2\pi y}{c}\Big]\omega^2 e^{-i\omega t}$

$e_{15}=\sum_{i=1}^{\aleph}\Big[\frac{\pi h_i}{3a}(2h_i-3)(\bar{Q}_{11}\alpha_{11}+\bar{Q}_{12}\alpha_{22})_i sin\frac{2\pi x}{a}\Big(1-cos\frac{2\pi y}{c}\Big)+\frac{2\pi h_i}{3a}(2h_i-3)(\bar{Q}_{16}\alpha_{11}+\bar{Q}_{26}\alpha_{22})_i\Big(1-cos\frac{2\pi x}{a}\Big)sin\frac{2\pi y}{c}\Big]$

$e_{16}=\sum_{i=1}^{\aleph}\Big[\frac{\pi h_i}{3b}(2h_i-3)(\bar{Q}_{12}\alpha_{11}+\bar{Q}_{22}\alpha_{22})_i\Big(1-cos\frac{2\pi x}{a}\Big)sin\frac{2\pi y}{c}+\frac{2\pi h_i}{3a}(2h_i-3)(\bar{Q}_{16}\alpha_{11}+\bar{Q}_{26}\alpha_{22})_i sin\frac{2\pi x}{a}\Big(1-cos\frac{2\pi y}{c}\Big)\Big]$

$f_1=\sum_{i=1}^{\aleph}\Big[-(\bar{Q}_{11})_i\frac{2\pi^2 h_i^2}{3a^2}\sin\frac{2\pi x}{a}\Big(1-\cos\frac{2\pi y}{c}\Big)+(2\bar{Q}_{16})_i\frac{2\pi^2 h_i^2}{3ac}\cos\frac{2\pi x}{a}\sin\frac{2\pi y}{c}+(\bar{Q}_{66})_i\frac{2\pi^2 h_i^2}{3c^2}\sin\frac{2\pi x}{a}\cos\frac{2\pi y}{c}\Big]e^{-i\omega t}$

$f_2=\sum_{i=1}^{\aleph}\Big[(\bar{Q}_{12}+\bar{Q}_{66})_i\frac{2\pi^2 h_i^2}{3ac}\sin\frac{2\pi x}{a}\cos\frac{2\pi y}{c}+(\bar{Q}_{16})_i\frac{2\pi^2 h_i^2}{3a^2}\cos\frac{2\pi x}{a}\sin\frac{2\pi y}{c}-(\bar{Q}_{26})_i\frac{2\pi^2 h_i^2}{3c^2}\Big(1-\cos\frac{2\pi x}{a}\Big)\sin\frac{2\pi y}{c}\Big]e^{-i\omega t}$

$f_3=\sum_{i=1}^{\aleph}\Big[-(\bar{Q}_{11})_i\frac{32\pi^3 h_i^3}{315a^3}\sin\frac{2\pi x}{a}\Big(1-\cos\frac{2\pi y}{c}\Big)-(\bar{Q}_{12}+2\bar{Q}_{66})_i\frac{32\pi^3 h_i^3}{315ab^2}\sin\frac{2\pi x}{a}cos\frac{2\pi y}{c}-(\bar{Q}_{16})_i\frac{32\pi^3 h_i^3}{315a^2c}\cos\frac{2\pi x}{a}\sin\frac{2\pi y}{c}+(\bar{Q}_{26})_i\frac{32\pi^3 h_i^3}{315c^3}\Big(1-\cos\frac{2\pi x}{a}\Big)\sin\frac{2\pi y}{c}+(\bar{Q}_{45})_i\frac{46\pi h_i}{15c}\Big(1-\cos\frac{2\pi x}{a}\Big)\sin\frac{2\pi y}{c}-(\bar{Q}_{55})_i\frac{46\pi h_i}{15a}\sin\frac{2\pi x}{a}\Big(1-\cos\frac{2\pi y}{c}\Big)\Big]e^{-i\omega t}$

$f_4=\sum_{i=1}^{\aleph}\Big[-(\bar{Q}_{11})_i\frac{4\pi^3 h_i^2}{3a^3}cos\frac{2\pi x}{a}\sin\frac{2\pi x}{a}\Big(1-\cos\frac{2\pi y}{c}\Big)^2+(\bar{Q}_{12})_i\frac{4\pi^3 h_i^2}{3ac^2}sin^2\frac{2\pi y}{c}\sin\frac{2\pi x}{a}\Big(1-\cos\frac{2\pi y}{c}\Big)-(\bar{Q}_{16})_i\frac{4\pi^3 h_i^2}{3a^2c}cos\frac{2\pi x}{a}\Big(1-cos\frac{2\pi x}{a}\Big)\sin\frac{2\pi y}{c}\Big(1-\cos\frac{2\pi y}{c}\Big)+(\bar{Q}_{16})_i\frac{4\pi^3 h_i^2}{3a^2c}sin^2\frac{2\pi x}{a}\sin\frac{2\pi y}{c}\Big(1-\cos\frac{2\pi y}{c}\Big)+(\bar{Q}_{26})_i\frac{4\pi^3 h_i^2}{3c^3}\Big(1-cos\frac{2\pi x}{a}\Big)^2 sin\frac{2\pi y}{c}cos\frac{2\pi y}{c}+(\bar{Q}_{66})_i\frac{4\pi^3 h_i^2}{3ac^2}\sin\frac{2\pi x}{a}\Big(1-cos\frac{2\pi x}{a}\Big)\Big(1-\cos\frac{2\pi y}{b}\Big)cos\frac{2\pi y}{c}\Big]e^{-2i\omega t}$

$f_5=\sum_{i=1}^{\aleph}\Big[-(\bar{Q}_{11})_i\frac{68\pi^2 h_i^3}{315a^2}\sin\frac{2\pi x}{a}\Big(1-\cos\frac{2\pi y}{c}\Big)+(\bar{Q}_{16})_i\frac{136\pi^2 h_i^3}{315ac}cos\frac{2\pi x}{a}\sin\frac{2\pi y}{c}+(\bar{Q}_{66})_i\frac{68\pi^2 h_i^3}{315c^2}\sin\frac{2\pi x}{a}cos\frac{2\pi y}{c}+(\bar{Q}_{55})_i\frac{23h_i}{15}\sin\frac{2\pi x}{a}\Big(1-\cos\frac{2\pi y}{c}\Big)\Big]e^{-i\omega t}$

$f_6 = \sum_{i=1}^{\aleph}\Big[(\bar{Q}_{12}+\bar{Q}_{66})_i \frac{68\pi^2 h_i^3}{315a^2}\sin\frac{2\pi x}{a}\cos\frac{2\pi y}{c} + (\bar{Q}_{16})_i \frac{68\pi^2 h_i^3}{315ac} cos\frac{2\pi x}{a}\sin\frac{2\pi y}{c} + (\bar{Q}_{26})_i \frac{68\pi^2 h_i^3}{315c^2}\left(1-\cos\frac{2\pi x}{a}\right) cos\frac{2\pi y}{c} + (\bar{Q}_{45})_i \frac{23h_i}{15}\left(1-\cos\frac{2\pi x}{a}\right)\sin\frac{2\pi y}{c}\Big] e^{-i\omega t}$

$f_7 = \sum_{i=1}^{\aleph}\left[I_{1i}\sin\frac{2\pi x}{a}\left(1-\cos\frac{2\pi y}{c}\right)\right]\omega^2 e^{-i\omega t}$

$f_8 = \sum_{i=1}^{\aleph}\left[\left(I_{2i}-\frac{8}{3h_i^2}I_{4i}+\frac{16}{9h_i^4}I_{6i}\right)\sin\frac{2\pi x}{a}\left(1-\cos\frac{2\pi y}{c}\right)\right]\omega^2 e^{-i\omega t}$

$f_9 = \sum_{i=1}^{\aleph}\left[\left(\frac{32\pi}{9ah_i^4}I_{6i}-\frac{8\pi}{3ah_i^2}I_{4i}\right)\sin\frac{2\pi x}{a}\left(1-\cos\frac{2\pi y}{c}\right)\right]\omega^2 e^{-i\omega t}$

$f_{10} = \sum_{i=1}^{\aleph}\left[\frac{h_i^2}{6}(\bar{Q}_{11}\alpha_{11}+\bar{Q}_{12}\alpha_{22})_i\right]$

$f_{11} = \sum_{i=1}^{\aleph}\left[\frac{h_i^2}{6}(\bar{Q}_{16}\alpha_{11}+\bar{Q}_{26}\alpha_{22})_i\right]$

$g_1 = \sum_{i=1}^{\aleph}\Big[(\bar{Q}_{12}+\bar{Q}_{66})_i \frac{2\pi^2 h_i^2}{3ac}\cos\frac{2\pi x}{a} sin\frac{2\pi y}{c} + (\bar{Q}_{26})_i \frac{2\pi^2 h_i^2}{3c^2}\sin\frac{2\pi x}{a}\cos\frac{2\pi y}{c} - (\bar{Q}_{16})_i \frac{2\pi^2 h_i^2}{3a^2}\sin\frac{2\pi x}{a}\left(1-\cos\frac{2\pi y}{c}\right)\Big] e^{-i\omega t}$

$g_2 = \sum_{i=1}^{\aleph}\Big[(2\bar{Q}_{26})_i \frac{2\pi^2 h_i^2}{3ac}\sin\frac{2\pi x}{a}\cos\frac{2\pi y}{c} + (\bar{Q}_{66})_i \frac{2\pi^2 h_i^2}{3a^2}\cos\frac{2\pi x}{a}\sin\frac{2\pi y}{c} - (\bar{Q}_{22})_i \frac{2\pi^2 h_i^2}{3c^2}\left(1-\cos\frac{2\pi x}{a}\right)\sin\frac{2\pi y}{c}\Big] e^{-i\omega t}$

$g_3 = \sum_{i=1}^{\aleph}\Big[(\bar{Q}_{12}-2\bar{Q}_{16})_i \frac{32\pi^3 h^3}{315a^2 c} cos\frac{2\pi x}{a} sin\frac{2\pi y}{c} + (\bar{Q}_{22})_i \frac{32\pi^3 h^3}{315c^3}\left(1-cos\frac{2\pi x}{a}\right)\sin\frac{2\pi y}{c} - (3\bar{Q}_{26})_i \frac{32\pi^3 h^3}{315ac^2} sin\frac{2\pi x}{a}\cos\frac{2\pi y}{c} - (\bar{Q}_{16})_i \frac{32\pi^3 h^3}{315a^3} sin\frac{2\pi x}{a}\left(1-\cos\frac{2\pi y}{c}\right) + (\bar{Q}_{44})_i \frac{46\pi h_i}{15c}\left(1-\cos\frac{2\pi x}{a}\right)\sin\frac{2\pi y}{c} + (\bar{Q}_{45})_i \frac{46\pi h_i}{15a} sin\frac{2\pi x}{a}\left(1-\cos\frac{2\pi y}{c}\right)\Big] e^{-i\omega t}$

$g_4 = \sum_{i=1}^{\aleph}\Big[(\bar{Q}_{12})_i \frac{4\pi^3 h_i^2}{3a^2 c}\sin^2\frac{2\pi x}{a} sin\frac{2\pi y}{b}\left(1-\cos\frac{2\pi y}{c}\right) + (\bar{Q}_{22})_i \frac{4\pi^3 h_i^2}{3c^3}\left(1-\cos\frac{2\pi x}{a}\right)^2\cos\frac{2\pi y}{c}\sin\frac{2\pi y}{c} + (\bar{Q}_{26})_i \frac{4\pi^3 h_i^2}{3ac^2} sin\frac{2\pi x}{a}\left(1-cos\frac{2\pi x}{a}\right)\left(1-\cos\frac{2\pi y}{c}\right)\cos\frac{2\pi y}{c} + (\bar{Q}_{16})_i \frac{4\pi^3 h_i^2}{3a^3} sin\frac{2\pi x}{a} cos\frac{2\pi x}{a}\left(1-\cos\frac{2\pi y}{c}\right)^2 + (\bar{Q}_{26})_i \frac{4\pi^3 h_i^2}{3ac^2} sin\frac{2\pi x}{a}\left(1-cos\frac{2\pi x}{a}\right) sin^2\frac{2\pi y}{c} - (\bar{Q}_{66})_i \frac{4\pi^3 h_i^2}{3a^2 c} cos\frac{2\pi x}{a}\left(1-cos\frac{2\pi x}{a}\right)\sin\frac{2\pi y}{c}\left(1-\cos\frac{2\pi y}{c}\right)\Big] e^{-2i\omega t}$

$g_5 = \sum_{i=1}^{\aleph}\Big[(\bar{Q}_{45})_i \frac{23h_i}{15} sin\frac{2\pi x}{a}\left(1-\cos\frac{2\pi y}{c}\right) + (\bar{Q}_{12}+\bar{Q}_{66})_i \frac{68\pi^2 h_i^3}{315ac} cos\frac{2\pi x}{a}\sin\frac{2\pi y}{c} + (\bar{Q}_{26})_i \frac{68\pi^2 h_i^3}{315c^2} sin\frac{2\pi x}{a}\cos\frac{2\pi y}{c} - (\bar{Q}_{16})_i \frac{68\pi^2 h_i^3}{315a^2} sin\frac{2\pi x}{a}\left(1-\cos\frac{2\pi y}{c}\right)\Big] e^{-i\omega t}$

$g_6 = \sum_{i=1}^{\aleph}\Big[(\bar{Q}_{44})_i \frac{23h_i}{15}\left(1-cos\frac{2\pi x}{a}\right)\sin\frac{2\pi y}{c} + (2\bar{Q}_{26})_i \frac{68\pi^2 h_i^3}{315ac} sin\frac{2\pi x}{a}\cos\frac{2\pi y}{c} + (\bar{Q}_{66})_i \frac{68\pi^2 h_i^3}{315a^2} cos\frac{2\pi x}{a}\sin\frac{2\pi y}{c} + (\bar{Q}_{22})_i \frac{68\pi^2 h_i^3}{315a^2}\left(1-cos\frac{2\pi x}{a}\right)\cos\frac{2\pi y}{c}\Big] e^{-i\omega t}$

$g_7 = \sum_{i=1}^{\aleph}\left[I_{1i}\left(1-\cos\frac{2\pi x}{a}\right)\sin\frac{2\pi y}{c}\right]\omega^2 e^{-i\omega t}$

$g_8 = \sum_{i=1}^{\aleph}\left[\left(I_{2i}-\frac{8}{3h_i^2}I_{4i}+\frac{16}{9h_i^4}I_{6i}\right)\left(1-\cos\frac{2\pi x}{a}\right)\sin\frac{2\pi y}{c}\right]\omega^2 e^{-i\omega t}$

$g_9 = \sum_{i=1}^{\aleph}\left[\left(\frac{32\pi}{9bh_i^4}I_{6i}-\frac{8\pi}{3bh_i^2}I_{4i}\right)\left(1-\cos\frac{2\pi x}{a}\right)\sin\frac{2\pi y}{c}\right]\omega^2 e^{-i\omega t}$

$g_{10} = \sum_{i=1}^{\aleph}\left[\frac{h_i^2}{6}(\bar{Q}_{12}\alpha_{11}+\bar{Q}_{22}\alpha_{22})_i\right]$

$g_{11} = \sum_{i=1}^{\aleph}\left[\frac{h_i^2}{6}(\bar{Q}_{16}\alpha_{11}+\bar{Q}_{26}\alpha_{22})_i\right]$

$\aleph$ is the number of layers and plies considered through the sandwich plate thickness.

Appendix B: Elements of Coefficient Matrix $[\chi]$

$$[\chi]_{5\times16} = \begin{bmatrix} c_1 & d_1 & 0 & f_1 & g_1 \\ c_2 & d_2 & 0 & f_2 & g_2 \\ c_3 & d_3 & e_5 & f_3 & g_3 \\ e^2c_4 & e^2d_4 & e^2e_6 & e^2f_4 & e^2g_4 \\ c_5 & d_5 & e_8 & f_5 & g_5 \\ c_6 & d_6 & e_9 & f_6 & g_6 \\ 0 & 0 & 0 & 0 & 0 \\ 0 & 0 & 0 & 0 & 0 \\ 0 & 0 & 0 & 0 & 0 \\ 0 & 0 & 0 & 0 & 0 \\ 0 & 0 & 0 & 0 & 0 \\ 0 & 0 & e^2e_1 & 0 & 0 \\ 0 & 0 & e^2e_2 & 0 & 0 \\ 0 & 0 & e^2e_3 & 0 & 0 \\ 0 & 0 & e^2e_4 & 0 & 0 \\ 0 & 0 & e^3e_7 & 0 & 0 \end{bmatrix}^{T}$$

Appendix C: Elements of Math Matrix $[M]$

$$[\mathrm{M}]_{5\times16} = \begin{bmatrix} 0 & 0 & 0 & 0 & 0 \\ 0 & 0 & 0 & 0 & 0 \\ 0 & 0 & 0 & 0 & 0 \\ 0 & 0 & 0 & 0 & 0 \\ 0 & 0 & 0 & 0 & 0 \\ 0 & 0 & 0 & 0 & 0 \\ -c_7 & 0 & e_{11} & -f_7 & 0 \\ 0 & -d_7 & e_{12} & 0 & -g_7 \\ -c_9 & -d_9 & -e_{10} & -f_9 & -g_9 \\ -c_8 & 0 & e_{13} & -f_8 & 0 \\ 0 & -d_8 & e_{14} & 0 & -g_8 \\ 0 & 0 & 0 & 0 & 0 \\ 0 & 0 & 0 & 0 & 0 \\ 0 & 0 & 0 & 0 & 0 \\ 0 & 0 & 0 & 0 & 0 \\ 0 & 0 & 0 & 0 & 0 \end{bmatrix}^{T}$$